EMG-BASED FORCE ESTIMATION USING DEEP LEARNING MODELS

By

Maham Nayab

(Registration No: 00000364006)

Department of Biomedical Engineering

School Of Mechanical & Manufacturing Engineering

National University of Sciences & Technology (NUST)

Islamabad, Pakistan

(2024)

EMG-BASED FORCE ESTIMATION USING DEEP LEARNING MODELS

By

Maham Nayab

(Registration No: 00000364006)

A thesis submitted to the National University of Sciences and Technology, Islamabad,

in partial fulfillment of the requirements for the degree of

Master of Science in
Biomedical Engineering

Supervisor: Dr. Asim Waris

School of Mechanical & Manufacturing Engineering

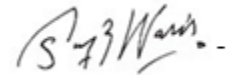National University of Sciences & Technology (NUST)

Islamabad, Pakistan

(2024)

THESIS ACCEPTANCE CERTIFICATE

Certified that final copy of MS Thesis written by Ms <u>Maham Nayab</u> (Registration No. <u>00000364006</u>), of <u>School of Mechanical & Manufacturing Engineering</u> (School/College/Institute) has been vetted by undersigned, found complete in all respects as per NUST Statutes/ Regulations/ Masters Policy, is free of plagiarism, errors, and mistakes and is accepted as partial fulfillment for award of Masters degree. It is further certified that necessary amendments as point out by GEC members and foreign/ local evaluators of the scholar have also been incorporated in the said thesis.

Signature:

Name of Supervisor: <u>Dr Muhammad Asim Waris</u>

Date: <u>February 12, 2024</u>

Signature (HOD):

Date: <u>February 12, 2024</u>

Signature (Dean/ Principal):

Date: <u>February 12, 2024</u>

National University of Sciences & Technology (NUST)
MASTER'S THESIS WORK

We hereby recommend that the dissertation prepared under our supervision by: Maham Nayab (00000364006)
Titled: EMG-BASED FORCE ESTIMATION USING DEEP LEARNING MODELS be accepted in partial fulfillment of the requirements for the award of MS in Biomedical Engineering degree.

Examination Committee Members

1.   Name: Muhammad Jawad Khan   Signature:

2.   Name: Adeeb Shehzad   Signature:

3.   Name: Aneeqa Noor   Signature:

Supervisor: Muhammad Asim Waris   Signature:

Date: 12 - Feb - 2024

                                              12 - Feb - 2024

Head of Department   Date

COUNTERSINGED

12 - Feb - 2024

Date   Dean/Principal

CERTIFICATE OF APPROVAL

This is to certify that the research work presented in this thesis, entitled "EMG-based force estimation using deep learning models" was conducted by MS Maham Nayab under the supervision of Dr Muhammad Asim Waris.
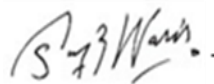
No part of this thesis has been submitted anywhere else for any other degree. This thesis is submitted to the Department of Biomedical Engineering in partial fulfillment of the requirements for the degree of Master of Science in Field of Biomedical Engineering

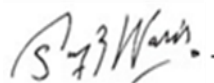Department of Biomedical Engineering and Sciences National University of Sciences and Technology, Islamabad.

Student Name: Maham Nayab   Signature: _____

Supervisor Name: Dr Muhammad Asim Waris   Signature: _____

Name of Dean/HOD: Dr Muhammad Asim Waris   Signature: _____

AUTHOR'S DECLARATION

I Maham Nayab hereby state that my MS thesis titled "EMG-based force estimation using deep learning models" is my own work and has not been submitted previously by me for taking any degree from National University of Sciences and Technology, Islamabad or anywhere else in the country/ world.

At any time if my statement is found to be incorrect even after I graduate, the university has the right to withdraw my MS degree.

Name of Student: Maham Nayab

Date: February 13, 2024

PLAGIARISM UNDERTAKING

I solemnly declare that research work presented in the thesis titled "EMG-based force estimation using deep learning models" is solely my research work with no significant contribution from any other person. Small contribution/ help wherever taken has been duly acknowledged and that complete thesis has been written by me.

I understand the zero tolerance policy of the HEC and National University of Sciences and Technology (NUST), Islamabad towards plagiarism. Therefore, I as an author of the above titled thesis declare that no portion of my thesis has been plagiarized and any material used as reference is properly referred/cited.

I undertake that if I am found guilty of any formal plagiarism in the above titled thesis even after award of MS degree, the University reserves the rights to withdraw/revoke my MS degree and that HEC and NUST, Islamabad has the right to publish my name on the HEC/University website on which names of students are placed who submitted plagiarized thesis.

Student Signature:

Name: Maham Nayab

To my beloved parents, Sajid Mehmood and Rehana Sajid, your collective wisdom, sacrifices, and boundless love are the bedrock of my aspirations.

To the remarkable women in STEM, whose brilliance and determination pave the way for future generations.

ACKNOWLEDGEMENTS

TABLE OF CONTENTS

LIST OF TABLES

LIST OF FIGURES

LIST OF SYMBOLS, ABBREVIATIONS AND ACRONYMS

EMG   Electromyography

sEMG   Surface Electromyography

iEMG   Intramuscular Electromyography

LSTM   Long Short Term Memory

GPR   Gaussian Process Regression

TCN   Temporal Convolutional Network

BPNN   Backpropagation Neural Network

TCN_LSTM   Hybrid Architecture of Temporal Convolutional Network and Long Short Term Memory

MLP   Multilayer Perceptron

cSVM   Cubic Support Vector Machine

NNN   Narrow Neural Network

MNN   Medium Neural Network

MAE   Mean Absolute Error

RMSE   Root Mean Square Error

R^2 Coefficient Of Determination

MSE   Mean Square Error

ABSTRACT

The estimation of force through electromyography (EMG) assumes paramount importance in diverse domains, including neurorehabilitation, myoelectric control, and neurofeedback systems. The intricate relationship between muscle contraction and force, characterized by linear associations in small muscles with narrow motor units and nonlinear relationships in larger muscles with wider motor units, underscores the complexity of this physiological interplay. Against the backdrop of a global demand for advanced technologies to address limb loss limitations, with an estimated 100 million individuals worldwide in need of prosthetics, there arises an urgent need for sophisticated solutions. Meeting the diverse needs of prosthetic users emphasizes the crucial role of EMG-based force prediction, striving to provide adaptive and personalized solutions for an inclusive and effective approach to limb rehabilitation. This comprehensive study explores the dynamic interplay between surface electromyography (sEMG) and intramuscular electromyography (iEMG) signals and force estimation. Leveraging a diverse set of machine learning and deep learning models, the research aims to predict forces in both healthy individuals and those with trans-radial amputations. Across sEMG and iEMG modalities, deep learning models, including Long Short-Term Memory (LSTM), Temporal Convolutional Network (TCN), and the hybrid LSTM-TCN, consistently exhibit remarkable efficacy. These models, boasting R^2 values surpassing 0.90 in force prediction, offer promising advancements in refining force estimation through electromyography. Notably, the TCN emerges as an exemplary performer, yielding R^2 values of 0.98 for able-bodied individuals and 0.87 for amputees in sEMG. Simultaneously, the hybrid TCN-LSTM model maintains strong performance with R^2 values of 0.98 for able-bodied individuals and 0.85 for amputees in sEMG. The LSTM model also upholds notable performance, showcasing R^2 values of 0.99 for able-bodied individuals and 0.80 for amputees in sEMG. Beyond unraveling the intricacies of EMG-based force estimation, this study sheds light on the unique challenges posed by amputations, contributing substantively to the ongoing quest for enhanced precision and effectiveness in rehabilitation interventions.

Keywords: Electromyography Signal, EMG based force estimation, Long Short-Term Memory (LSTM), Temporal Convolutional Network (TCN), Trans-Radial amputation

CHAPTER 1:   INTRODUCTION

2.1 Background

The field of Human-Machine Interaction (HMI) faces a significant challenge in the estimation of gripping force from electromyography (EMG) signals. This challenge holds crucial implications for developing interfaces that facilitate fluent and precise control of robots based on EMG inputs. While EMG signals generated by human hand movements are commonly employed for accurate decoding of different action types, existing classifications of gestures often overlook the impact of force dynamics. Specifically, the estimation of grasp force during natural grasping movements has been an area of neglect. Addressing this gap is essential as it could significantly enhance the accuracy of prosthesis control systems.

In addition to prosthesis control, there is a broader need for accurate force estimation, particularly in strength training exercises such as biceps curls. The feedback of muscle force levels is pivotal in improving the quality of strength training workouts. Beyond the direct measurement of end-point force levels at the hand during exercises, surface electromyography (EMG) signals emerge as a valuable source of force information related to the biceps muscle. Various methods, including biomechanical models like the Hill-type model, have been proposed to estimate force levels from EMG signals. However, despite these advancements, accurately modeling the intricate and person-specific relationship between EMG and force remains a challenging problem.

2.2 Research Problem

The core research problem centers around the accurate estimation of force or torque generated by muscle contractions, particularly in the context of EMG signals. The nonlinear, dynamically changing, and person-specific nature of the EMG–force relationship poses a substantial challenge in developing an accurate model that can generalize across participants. The research aims to address this problem by exploring different approaches, including physiologically based models such as Hill's muscle model and activation-based models, to enhance the accuracy and applicability of force estimation from EMG signals.

2.3 Objective

This research endeavors to delve into the realm of electromyography (EMG) signals for force prediction, aiming to contribute valuable insights into the comparative effectiveness of such signals in both healthy and amputee subjects. The primary objective is to rigorously investigate and compare the accuracy and precision of force prediction, utilizing EMG data from surface electromyography (sEMG) and intramuscular electromyography (iEMG). By scrutinizing the effectiveness of these EMG modalities, the study seeks to uncover their unique contributions to predicting forces in diverse populations. Moreover, the research extends its focus to the development and validation of enhanced force prediction models. The innovative approach involves integrating insights derived from both sEMG and iEMG data, recognizing the potential synergy in combining these complementary sources of information. The ultimate goal is to refine and validate models that not only improve precision but also exhibit heightened applicability in both healthy and amputee individuals.

CHAPTER 2:   LITERATURE REVIEW

Electromyograph signals are the measure of electrical current generated in the muscle during contraction and relaxation.
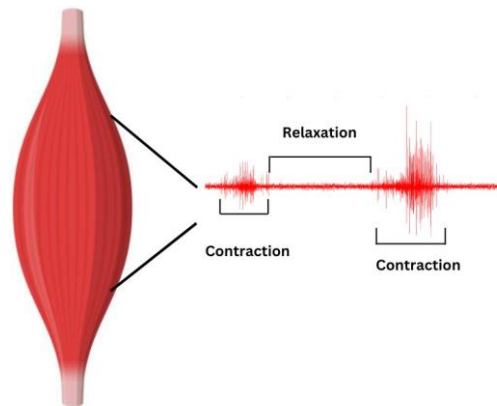
Figure 2.1 Muscle and its EMG signal

2.1 Motor unit and motor unit potentials

A motor unit (MU) is the essential working unit in our neuromuscular system. It consists of an alpha-motoneuron and the group of muscle fibers it controls. These MUs can vary significantly in size, depending on the number and size of the muscle fibers they connect to.
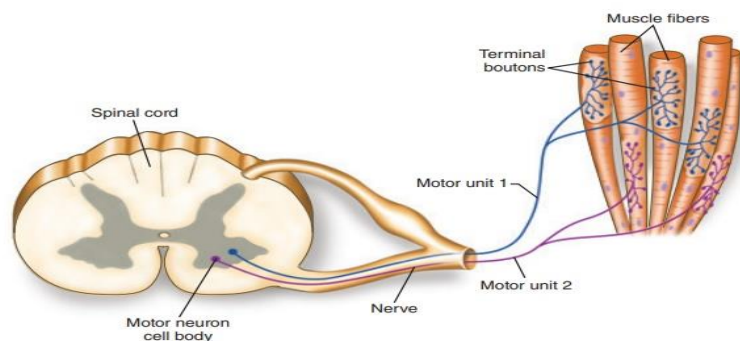
Figure 2.2 Motor unit is composed of motor neurons and all the muscle fibers.

When you want to move a muscle, like lifting your arm, your brain sends an electrical signal down a nerve to the muscle. This signal, or action potential, travels from the nerve cell's body to the ends

of its branches, which connect to the muscle fibers. At these connections, called neuromuscular junctions, the action potential triggers the muscle fibers to contract. This is how muscle movement begins. When the muscle fibers get this signal, they generate two action potentials that travel in opposite directions along the muscle fiber. These action potentials travel until they reach the ends of the muscle fiber, where they create a kind of electrical standing wave, marking the end of this electrical cycle in the muscle. This whole process creates a changing electrical current within the muscle, which produces changes in the area around the muscle. Electrical signals are conducted by the tissues of muscles just like how electric potentials are generated by the nerves in the nervous system. There are two types of electromyography signals: Surface Electromyograph and intramuscular electromyography. Intramuscular electromyography is an invasive EMG recording method. The signals are recorded by inserting a fine wire electrode into the muscle via skin. Surface Electromyography is a noninvasive method of recording the signal using surface electrodes. The surface electrodes are placed on the skin above the muscle with the help of gel.

Figure 2.3 Surface and intramuscular electrodes

Each muscle fiber within a motor unit is linked to the central nervous system. This means that motor units work together as a functional team. They all have similar characteristics in terms of how they respond to electrical signals and how they function. The 'size principle' determines how motor units are recruited. When you need more force, your body activates motor units starting with the smaller, weaker ones and then moving up to the larger, stronger ones. This process ensures that your muscles can produce the right amount of force for the task at hand.

In EMG, what you see on the skin's surface is the combined effect of all the motor unit action potentials (MUPs). These MUPs are like the basic building blocks of the EMG signal, and they

provide information about how your muscles are working and which motor units are being used when you move or perform tasks. The EMG signal at any given time can be either positive voltage or negative voltage. The useful frequency range of an EMG signal is between 0 to 500 Hz. The amplitude ranges from 5 to -5 mV before any amplification. While the EMG signal is being recorded and its journey through various tissues, it picks up unwanted noise. There are different types of noises affecting electromyography that are inherent electronic noise, ambient noise, motion artifact, and inherent signal stability electronic equipment generates noise, which, unfortunately, cannot be eliminated. The use of high-quality electronic components can only minimize this type of power line noise. Electromagnetic radiation is a significant source of ambient noise. Our bodies are continuously exposed to electromagnetic radiation, making it nearly impossible to avoid. Ambient noise can have amplitudes of one to three orders of magnitude greater than the EMG signal itself. Motion artifacts can distort the EMG signal, resulting in irregularities in the data. It primarily originates from two sources: the electrode interface and the electrode cable.
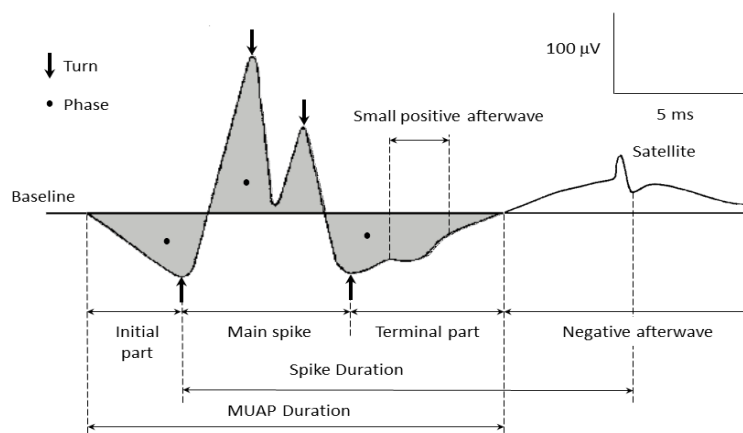
Figure 2.4 Parts of EMG signal

Proper design of the electronic circuitry and setup can help reduce motion artifacts.EMG signal amplitudes exhibit a random nature. This noise in the signal is primarily due to the firing rate of motor units, which typically operate in the frequency range of 0 to 20 Hz. This type of noise is called inherent signal stability.
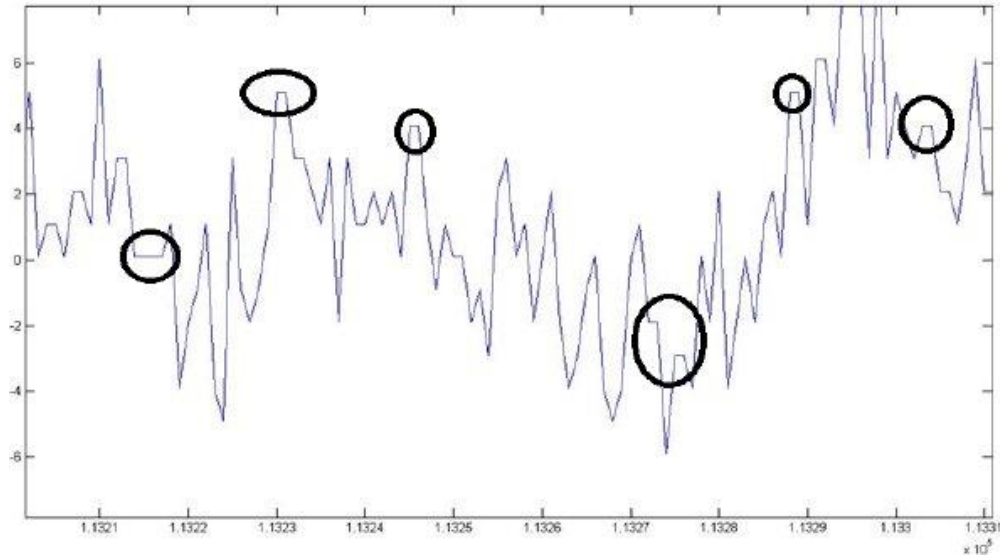
Figure 2.5 Different kind of noises in an EMG signal

2.2 Factors affecting EMG signal.

To understand the factors that influence the quality of electromyography (EMG) signals, we can categorize them into three main groups: causative factors, intermediate factors, and deterministic factors. Causative factors have a direct impact on the signals and can be divided into two subcategories. Extrinsic causative factors relating to the structure and placement of electrodes used in EMG measurements. These include considerations such as the size and shape of the electrodes, the distance between them, and their precise location concerning motor points within the muscle. Intrinsic causative factors, on the other hand, are influenced by physiological, anatomical, and biochemical aspects. These encompass factors like the number of active motor units, the composition of muscle fiber types, blood flow, fiber diameter, depth, and the tissue between the muscle surface and the electrode. Intermediate factors represent physical and physiological phenomena influenced by one or more causative factors. These factors may involve aspects like the band-pass filtering characteristics of the electrodes and their detection volume, the superposition of action potentials within the recorded EMG signal, and the conduction velocity of action potentials along the muscle fiber membrane. Additionally, crosstalk from nearby muscles can be considered an intermediate factor, as it affects the recorded EMG signal. Deterministic factors are influenced by intermediate factors and encompass elements such as the number of active motor units, the rate at which motor units fire, and the mechanical interactions between

6

muscle fibers. The amplitude, duration, and shape of motor unit action potentials also play a role in determining the quality of the EMG signal.

To optimize the quality of EMG signals, it is essential to consider several key practices. Maximizing the signal-to-noise ratio is crucial to preserve as much information from the EMG signal as possible while minimizing noise contamination. Distortion of the EMG signal should be minimized by avoiding unnecessary filtering, with a general recommendation against using notch filters. During the processing of EMG signals, the analysis of only positive values can be advantageous. This can be achieved through half-wave rectification, which removes negative data, or full-wave rectification, which uses the absolute value of each data point. Typically, full-wave rectification is preferred in EMG signal processing to enhance signal quality and extract meaningful information.

2.3 Relationship between EMG and force

When a muscle contracts, it also generates a force signal. There are three factors influencing muscle force: number of active MUs, their size, and their firing rate. For the estimation of force, spatial and temporal information. Spatial information is related to active Mus and temporal information is related to firing rates of MUs. Together they are referred to as muscle activation. Muscle activation is an abstract, time-varying model input variable that scales the ultimate model output: muscle force. It is estimated using the amplitude of electromyography signal amplitude. This amplitude is influenced by various aspects, including MU size, the number of active MUs, and their firing rates. However, because this amplitude is a one-dimensional signal, it can only provide an imperfect representation of all three critical factors. The force generated by a single motor unit is regulated by its firing rate. When an alpha motor neuron initiates an action potential, it leads to the generation of motor unit potential. The motor unit then generates a monophasic contraction named twitch. Twitch exerts tensile force lasting from fifty to one hundred and fifty milliseconds. This duration is significantly longer than the duration of the MUP as recorded with sEMG. Because of the longer twitch duration, twitches from different MUs will overlap and summate, even at low MU firing rates. This overlapping and summation of twitches are what leads to a functionally relevant increase in force as the firing rate of MUs increases. This increase in force reaches a saturation point at around 30 to 40 pulses per second, which is below the maximum

MU firing rate. When the firing rate exceeds this point, it begins to affect the EMG signal and can compromise the accuracy of force estimation Firing rates above 40 pulses per second are known to be more useful for controlling the rate of force development rather than the overall force output. While some models, like the forward dynamic model for wrist movement driven by EMG signals, consider the dynamics of muscle activation, many models assume a direct (albeit time-delayed) relationship between EMG and muscle force. In cases where high firing rates are involved, doublet MUPs, which are essentially two MUPs occurring very close together in time (within 20 milliseconds), have been observed, especially at the initiation of fast movements. Although doublets are brief and occur in only a limited number of MUs, they can contribute to an overshoot in force predictions derived from EMG, particularly at the onset of a contraction.
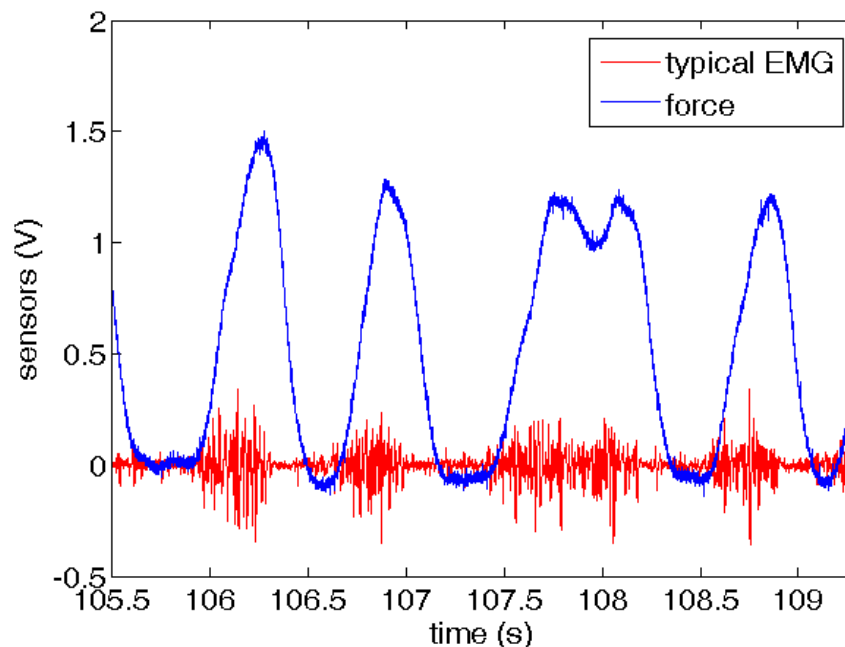
Figure 2.6 EMG and Force signal recorded simultaneously [8].

2.4 EMG-based Force Estimation

Accurate EMG-based force estimation is integral for many fields and applications like robotics, prosthesis control, rehabilitation, sports, and clinical diagnostics. Since 1950, scientists have used EMG for the estimation of force [2]. The relationship between force and EMG varies from subject to subject and is nonlinear and quite complex. Over the years, many scientists have proposed

8

different models for the prediction of force but there is still a more accurate model. Physiological models and data-driven models are the two main types of models that are used for the estimation of force [3]. Physiological models include models like Hills muscle models and musculoskeletal models where the biomechanical properties of muscles are required for force prediction. However, the physiological models have limitations since the performance of these models is dependent upon the accuracy of the physiological parameter estimated and their suitability as some parameters can't be measured experimentally [4-8]. Another study introduces a multi-scale physiological model for EMG-based force estimation, incorporating neural activation frequency and force-velocity properties. Results indicate that this model outperforms traditional Hill models, offering enhanced accuracy across a wider range of contraction conditions [16]. Data-driven models are machine learning or deep learning models that are given EMG as input and estimate the force. In 2019, Ali Ameri et al proposed convolutional neural networks as a model for force estimation[9]. The study demonstrates the inaugural validation of a regression CNN model for online Fitts' law-style tests involving individual and simultaneous wrist motions, surpassing a support vector regression-based system in throughput, especially with high EMG amplitudes. These findings underscore the CNN model's ability to extract motor control information from EMG signals for both single and multiple degree-of-freedom tasks, offering independent and simultaneous motion control, and distinguishing it from prior classification CNN models[9].In 2021 Gelareh Hajian et al proposed multimodal deep CNN for EMG-based force estimation. Their proposed model extracts EMG and IMU data to create effective force estimation embeddings, evaluated on a new dataset across diverse experimental conditions. Results demonstrate robustness, with R^2 values ranging from 0.59 to 0.91, highlighting significant improvement in force estimation when including kinematic information [3]. In another study, Gelareh Hajian explores channel selection methods for enhancing force estimation using the FOS algorithm with sEMG signals from biceps brachii and brachioradialis. It introduces a novel approach based on high PSD mean and low cross-correlations among channels, resulting in improved force estimates compared to using all available channels [10]. Hashemi, Javad, et al researched to observe the effect of angle-based EMG amplitude calibration and parallel cascade identification (PCI) modeling on EMG-based force estimation and observed Lower force estimation errors [11]. In another study, Hashemi, Javad, et al proposed a calibration method to address SEMG amplitude changes with joint angle. Calibrated models show a significant improvement in force estimation,

indicating the method's effectiveness in compensating for SEMG-force relationship variations with changing joint angles, reducing the need for nonlinear, joint angle-dependent terms in the model [21]. Another study proposed a nonnegative matrix factorization method to identify activation patterns as well as select EMG channels for force estimation. The method provides a way to find proper electrode placement for force estimation [14].

A study conducted in 2013 used the root mean square of the EMG signal as an input to support vector regression and autoregressive coefficient for emg-based force estimation[17]. Another study conducted used a linear regressor with a feature section to estimate early transient EMG from grasp force achieving an absolute error of 2.52% [12]. In another study, the mean frequency was calculated from cwt and was given as an input to the artificial neural network. A root means square error of 0.710 was observed by the researcher [13].In another study, J. Luo proposed a three-domain fuzzy neural network. Mean absolute values were used as an input of the model and an R^2 of 1 and an average mean square error of .0486 was observed [15]. Linfeng Chu in his study used a convolutional neural network, long short term memory, and hybrid architecture of CNN and LSTM for EMG-based force estimation and observed mean root mean square percentages of 12.13 ± 1.98, 9.07 ± 1.29, and 8.67 ± 1.14 respectively [18]. Changchang Wu proposes a generalized regression neural network as a model for EMG based forced estimation [19]. Another study proposes an adaptive method using EMG signals and radial basis function neural networks (RBFNNs) to estimate active joint torque for a lower limb robotic exoskeleton. The method enables practical and adaptive torque estimation, ensuring accurate exoskeleton movement control in both simulations and experiments, particularly during the swing phase [20]. Cao proposed Extreme machine learning as a model for force prediction and compared its performance with support vector regression and multiple nonlinear regression. ELM possesses relatively good accuracy and little consumed time, although SVM is effective for handgrip force estimation in terms of accuracy[22]. Yang Zheng used motor unit (MU) discharge data extracted from high-density EMG via Fast ICA to estimate isometric finger extension force in real time. Results demonstrated stable real-time MU decomposition accuracy (86%) and superior, stable force estimation using the neural-drive method compared to the EMG amplitude method during prolonged muscle contractions [23]. Yasheng Wu conducted a study to find differences in musculation using sEMG signal in the process of increasing and decreasing force and to create a model of the relationship between sEMG and force and concluded that the sEMG signal evoked

via musculation is not the same in the two processes, with a more significant difference when the muscle contraction strength is weaker, and a less significant [24]. Sakamoto, Sei-ichi, et al used EMG and imu data as an input to a long short-term memory to estimate ground reaction force and observed a root mean square error of 8,22 and 11.17 for posture control motion and stepping motion [25]. He Mao proposed a hybrid EMG and acceleration multimodal scheme for the estimation of force and wrist angles and observed an R^2 of 97.18±0.96% [26]. In another study, He Mao proposed a hybrid Generalized neural network and multilinear regression model and observed $R^2 = 96.33 \pm 1.13\%$ and MAE= $2.11 \pm 0.52\%$ for the intact subjects, and $R^2 = 86.86\%$ and MAE= 2.13% for the amputee [27]. Another study examines the applicability of HD-sEMG for force prediction in ecologically relevant conditions using four input force profiles. It finds that the crest factor of input signals significantly affects the performance of EMG-Force models, with the minimum crest factor signal showing the best results, underscoring the importance of considering this parameter during model training [28]. Xinyu Jiang proposed to employ a forest ensemble model and observed an R^2 of 95.12 % [29]. A study was conducted to investigate the Long Short-Term Memory (LSTM) network for the kinetics and kinematics prediction of human lower limbs when performing different activities without using force plates after the learning and average R^2 scores for knee angle was 97.25%, knee moment was 94.9%, ankle angle was 91.44%, and ankle moment was 85.44% [30].

CHAPTER 3: METHODOLOGY

In this study, two databases were utilized. One was a self-acquired dataset, and the other was a publicly available dataset. The publicly available dataset in this study was downloaded from an online database named DB3 available on the website Ninapro [30]. The data consists of the simultaneously acquired data of both electromyography and force signals. And data is acquired from 11 trans-radial amputees.

3.1 Publicly available dataset

3.1.1 Electromyography Signal

The EMG data was acquired using Delsys double differential sEMG electrodes in the database. The data was acquired from 12 muscles using 12 Trigno wireless electrodes.

Figure 3.1 Delsys Trigno Delsys and Its double differential sEMG electrodes

Each electrode is equipped with a self-contained rechargeable battery and can operate within a range of 40 meters. These electrodes also come with a wireless receiving base station. The sEMG (surface electromyography) signals are recorded at a sampling rate of approximately 2,000 samples per second, and they exhibit a baseline noise level of less than 750 nanovolts RMS. Additionally, these electrodes are equipped with 3-axis accelerometers that sample data at a rate of 148 samples per second. To facilitate acquisition, the electrodes are affixed to the forearm using the standard adhesive bands provided by the manufacturer. To ensure secure placement during data collection, a hypoallergenic elastic latex-free band is applied around the electrodes. Eight electrodes are

evenly distributed around the forearm, situated at the level of the radio-humeral joint. Two additional electrodes are positioned on the primary active regions of the flexor digitorum superficialis and extensor digitorum superficialis muscles. In the second configuration, two more electrodes are added to target the primary active areas of the biceps brachii and triceps brachii muscles. These critical muscle activity sites were determined through palpation.
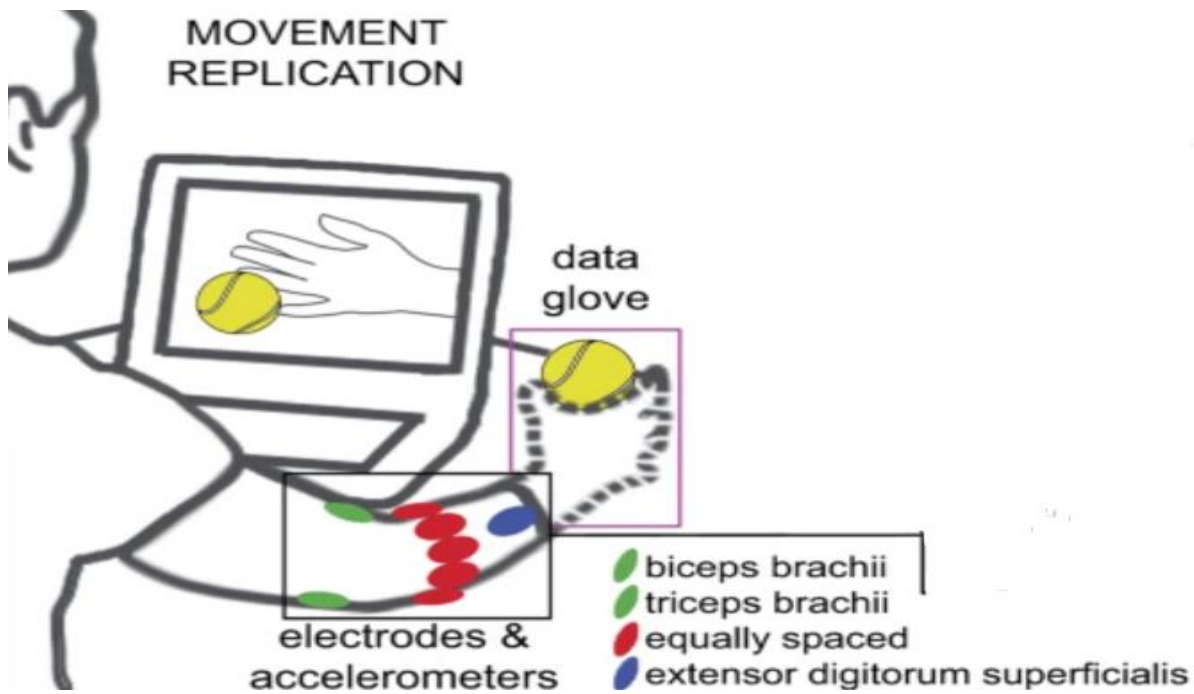
Figure 3.2 Electrode Placement in db3

3.1.2   Force Signal

Force signal was acquired using a Finger force linear sensor. Koiva, Risto, Barbara Hilsenbeck, and Claudio Castellini developed this device in 2012[31]. Accommodating various hand sizes, the FFLS ensures precision with up to 100N force measurement for each finger and a total of 200N, providing a linear signal response within the ±10V range. Strain gauge sensors from ME-Meßsysteme GmbH and Honigmann Industrielle Elektronik GmbH, along with custom bolts and adjustable hook-and-loop bands, secure the fingers to the sensors. The FFLS's reliability and precision were validated through testing, demonstrating its effectiveness within the physiological range..
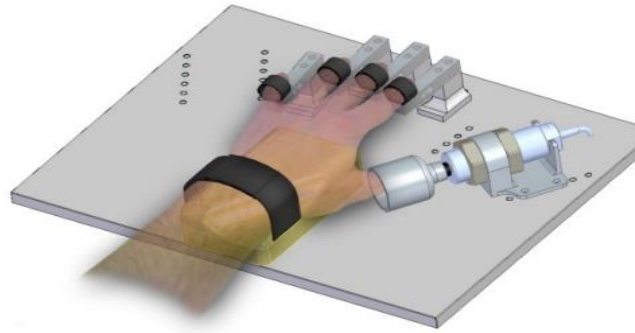
Figure 3.3 Finger force Linear Sensor

3.1.3   Protocol

In this study, individuals with abled bodies were instructed to experiment using their right hand, while amputated individuals were asked to mentally replicate the movements as naturally as possible with their missing limb. It is crucial to note that amputees, as a rule, cannot provide reliable ground truth data since they cannot operate any sensors with their missing limbs. To address this inherent challenge, previous research has employed two primary approaches: (a) instructing subjects to perform a task bilaterally while recording the ground truth data from the abled limb or (b) instructing subjects to follow a visual stimulus. There is no consensus on the optimal procedure, so each amputee participant was given the freedom to choose their preferred approach following a brief training phase. Consequently, only two subjects opted for bilateral execution, resulting in the database containing solely the visual stimulus as the ground truth reference. Nevertheless, it is worth noting that analyses using the visual stimulus as ground truth have already yielded successful results in previous work. The figure 3.4 shows the nine-force pattern used in this study.

3.2 Self-Acquired Dataset

3.2.1   Subjects

This study was a collaborative effort with King's College London, where the data acquisition process was conducted. The study involved 10 able-bodied participants, comprising six men and four women, with ages ranging from 23 to 26 years. All protocols strictly adhered to the principles outlined in the Declaration of Helsinki and received approval from the Danish Local Ethical

Committee (approval no. N-20080045). Before participating in the experimental procedures, subjects provided written and informed consent. Importantly, none of the participants had a history of upper extremity or other musculoskeletal disorders.

3.2.2 Force Signal

Customized hand support, incorporating a commercially available dynamometer (Gamma FT-130-10; ATI Industrial Automation, Apex, NC), provided subjects with feedback on activation levels for each task. Two torque signals, corresponding to the two Degrees of Freedom (DoF), were recorded.

3.2.3 EMG Signal

Six pairs of surface EMG electrodes were equally placed around the forearm, starting a few centimeters laterally to the ulnar exposure at the point of the largest circumference. Intramuscular EMG was captured using six bipolar wire electrodes, inserted underneath each surface EMG electrode pair, ensuring an equidistant distribution around the forearm. Teflon-coated stainless steel wire electrodes were inserted into each muscle with a sterile, 25-gauge hypodermic needle.

Flexion of little finger   Flexion of ring finger   Flexion of middle finger   Flexion of index finger

Abduction of thumb   Flexion of thumb   Flexion of index and little finger   Flexion of middle and little finger

Flexion of thumb and index finger
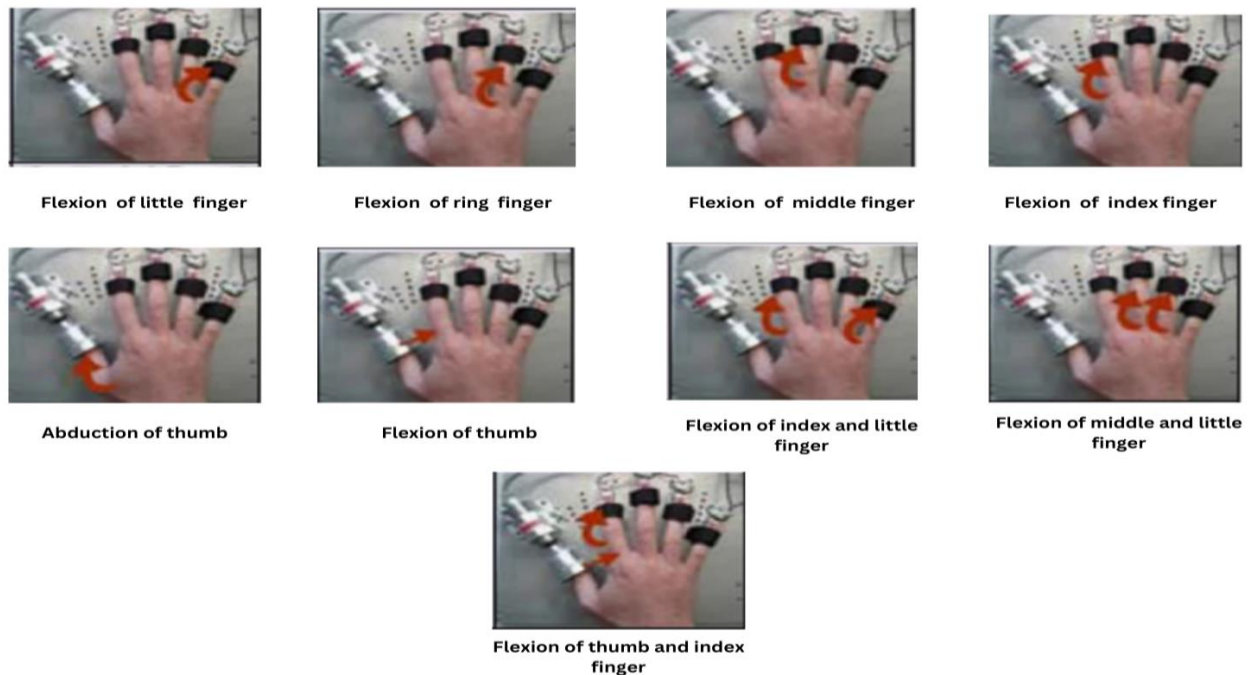
Figure 3.4 Force pattern followed in study

The insulated wires, exposing only the cross-section at the tip, provided high selectivity, typically encompassing up to 14 Motor Units (MUs) at 10–12% maximum voluntary The needle, inserted to a depth of 10–15 mm below the muscle fascia, was then removed, leaving the wire electrodes inside the muscle. To maintain consistency with prior force estimation studies only the end of the wires was exposed, ensuring high selectivity. A reference electrode was positioned around the wrist. All signals underwent anti-alias filtering and amplification and were sampled at 10 kHz.

EMG and torque signals were collected during isometric contractions, simulating two wrist Degrees of Freedom (DoF). The experiment comprised two trials with a 5-minute rest interval, each involving six task combinations. These tasks, categorized into individual and simultaneous DoF, aimed to assess torque estimation in isolated and dual DoF settings. The chosen DoFs were wrist flexion/extension (DoF1) and wrist supination/pronation (DoF2). Tasks included wrist flexion/extension, supination/pronation, and simultaneous flexion-pronation/extension-supination. The study focused on two DoFs, mirroring the limitations of current prosthetic devices. Tasks followed a dynamic, sinusoidal profile lasting 30 seconds with maximum amplitudes of 3 Nm for men and 2 Nm for women. Torque levels for female subjects were capped at 2 Nm due to comfort concerns, while 3 Nm was adopted for comparable EMG activation in females. Each 30-second profile began and ended with a rest period. To induce dynamic contractions necessitating constant torque and EMG intensity changes, sinusoidal profiles were employed. Subjects, seated with their right arm on an armrest and left arm relaxed on the table, tracked one or two simultaneous profiles based on the task. The task order was randomized, with visual feedback provided for accuracy. Subjects received ample training time to familiarize themselves with the profiles. Profile frequency was set at 0.5 Hz. Figure 3.6 shows the workflow of study

Figure 3.5 Ot Bioelectronica EMG USB2+

3.3 Data Preprocessing

After the data was downloaded, the EMG and force data both were preprocessed to get rid of noise and artifacts. To remove the power line interference, we used a notch filter with a cutoff frequency of 50Hz for both EMG and force signals. For the EMG signal, a fourth-order Butterworth bandpass filter with a lower cutoff frequency of 500 and a higher cutoff frequency of 20 was applied. For force signal, a fourth-order Butterworth lowpass filter with a lower cutoff frequency of 20 HZ was applied. Both the electromyographic (EMG) signals, including surface EMG (sEMG) and intramuscular EMG (iEMG), along with the force signal, were segmented into overlapping segments of 300 ms duration with a 50% overlap. Figure 3.7-3.13 shows the time and frequency spectrum of raw and filtered EMG and force signal.
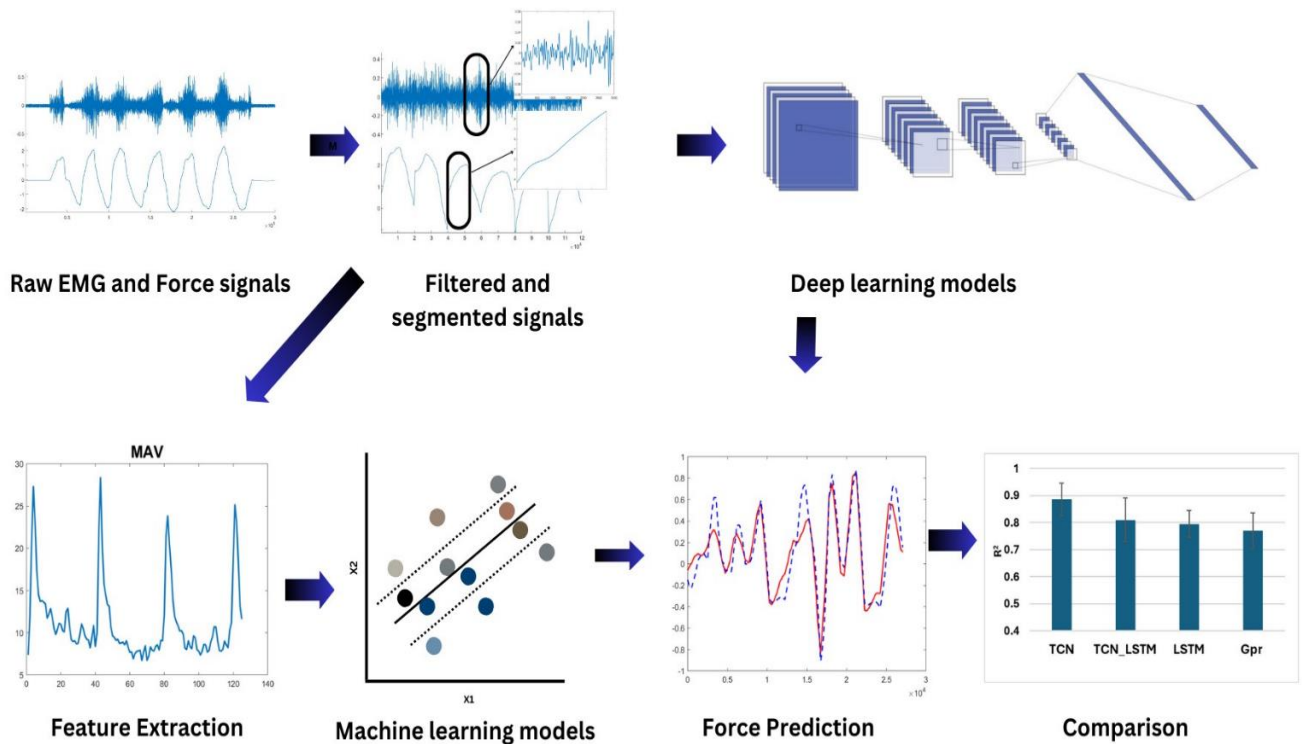
Figure 3.6 Workflow of the study.
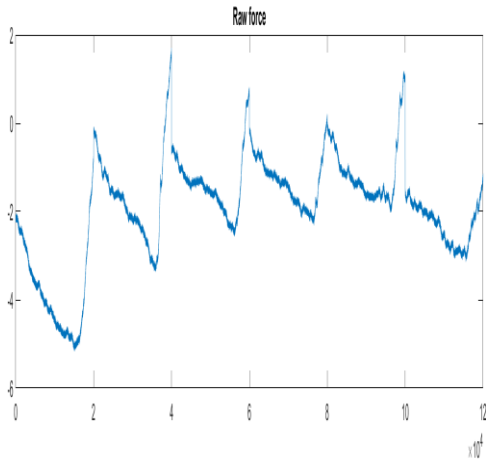
Figure 3.7 Raw force
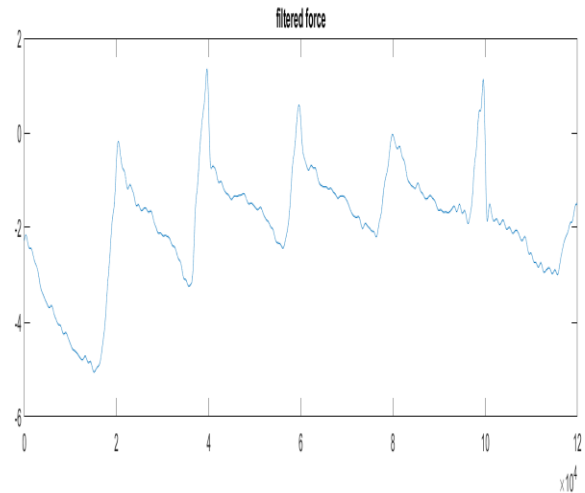
Figure 3.8 Filtered force signal.
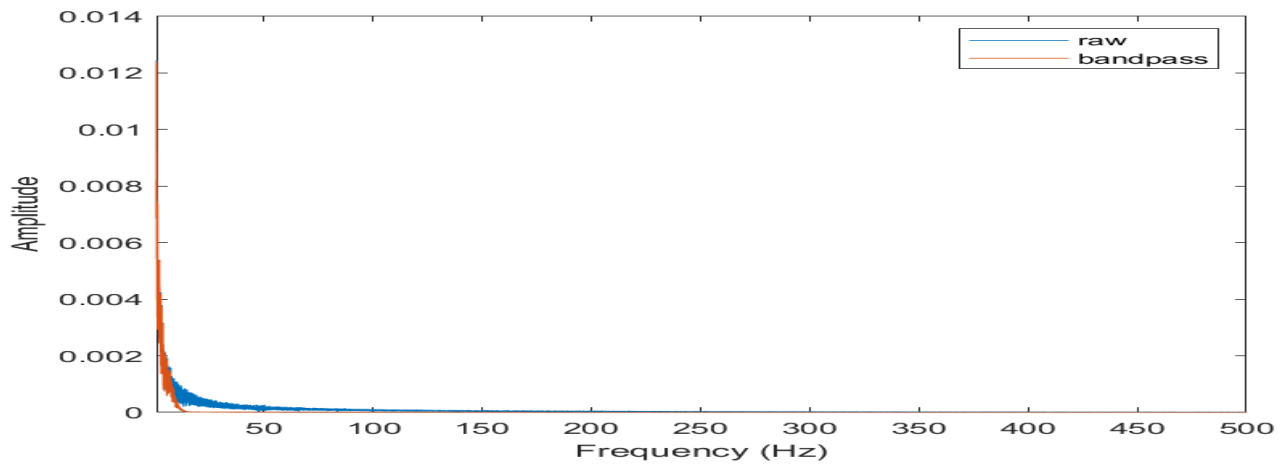
Figure 3.9 Frequency spectrum of Raw and filtered force signal.
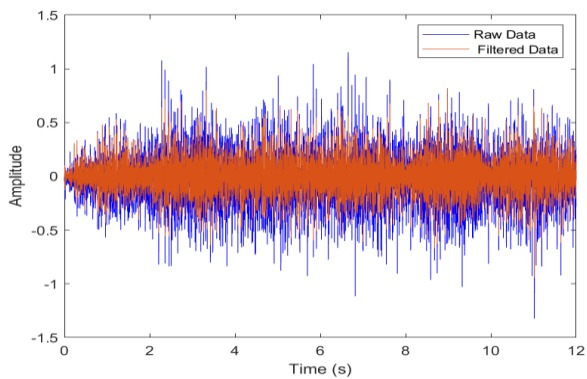
Figure 3.10 Raw and filtered sEMG signal.
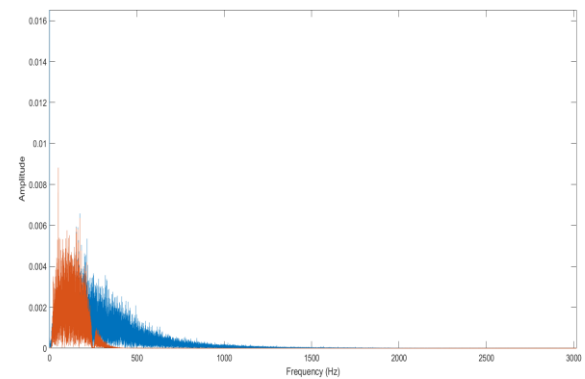
Figure 3.11 Frequency spectrum of both raw and filtered signal.
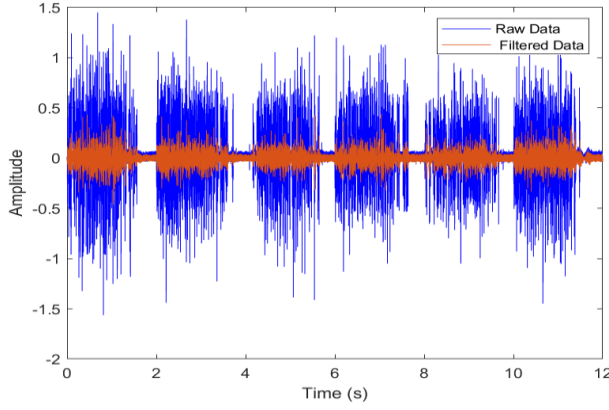
Figure 3.12 Raw and filtered iEMG signal,
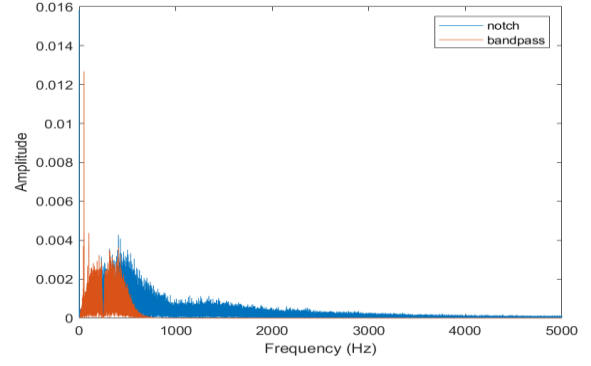
Figure 3.13 Frequency spectrum of both raw and filtered signal.

3.4 Feature Extraction

After segmentation feature extraction was done for machine learning models, segmented signal was given directly as an input to the Deep learning models. 13 time domain features were extracted from the segmented sEMG and iEMG signal.

Table 3.1 Features and their mathematical expressions.

Sr No	Features	Mathematical expressions
1	Difference Absolute Mean Value	$DAMV = \frac{1}{M-1} \sum_{j=1}^{M-1} \|z_{j+1} - z_j\|$ [34,33]
2	Log Difference Absolute Mean Value	$LDAMV = \sum_{j=1}^{M-1} \|z_{j+1} - z_j$ [35]
3	Mean Absolute Value	$MAV = \frac{1}{M} \sum_{j=1}^{M} \|z_j\|$ [32]
4	Modified Mean Absolute Value	$MAV1 = \frac{1}{M} \sum_{J=1}^{M} x_J \|Z_J\|$ [37] $x_j = \begin{cases} 1, & if\ 0.25N \leq I \leq 0.75N \\ 0 & otherwise \end{cases}$

19

5	Waveform Length	$WL = \sum_{j=1}^{M-1}\left|z_{j+1} - z_j\right|$ [36]
6	Standard Deviation	$\sigma = \sqrt{\frac{\sum z_j - Me^2}{M}}$ [37]
7	Root Mean Square	$RMS = \sqrt{\frac{1}{M}\sum_{j=1}^{M} z_j^2}$ [37]
8	Absolute Value Of The Summation Of Square Root	$AVSR = \left|\sum_{j=1}^{M} z_j^{1/2}\right|$ [28]
9	Mean Absolute Deviation	$MAD = median\left(\left|Z_i - \tilde{Z}\right|\right)$
10	Integral Absolute Value	$IAV = \sum_{i=1}^{M}\left|x_i\right|$ [31]
11	Interquartile Range	IQR = Q3 - Q1 [30]
12	Maximum Fractal Length	$MFL = Log_{10}(\sqrt{\sum_{j=1}^{M-1}\left(z_{j+1} - z_j\right)^2}$ [40]
13	V Order	$V = \left(\frac{1}{M}\sum_{j=1}^{M} z_j^v\right)^{\frac{1}{v}}$ [39]

3.5 Models for force prediction

Force prediction is done using Regression models. In this study we are using a variety of machine learning, deep learning, and shallow neural networks. Gaussian process regression (Gpr), cubic support vector machine (cSVM), medium neural network (MNN), narrow neural network (NNN), multilayer perceptron (Mlp), backpropagational neural network (BPNN), long short term memory (LSTM), Temporal convolutional network (TCN) and hybrid architecture of both TCN and LSTM.

3.5.1 Temporal Convolutional Network (TCN)

Temporal Convolutional Neural Networks (TCNs) stand as versatile convolutional networks designed specifically for sequence modeling tasks, enforcing a causal constraint. In the context of an input sequence (x_0 to x_t) and its corresponding output sequence (y_0 to y_t), a sequence modeling network is trained to predict the output sequence ($\hat{y}_0$ to $\hat{y}_t$) based on a defined loss function. The crucial causal constraint dictates that the prediction $\hat{y}_t$ solely relies on the past inputs (x_0 to x_t) and remains independent of future inputs (x_{t+1} to x^T). Temporal Convolutional Networks (TCNs) distinguish themselves with two key features: firstly, the use of causal convolutions, preventing information leakage from the future to the past; and secondly, the ability to handle sequences of variable lengths, aligning with the functionality of Recurrent Neural Networks (RNNs). Beyond these attributes, the emphasis is on constructing extensive effective history sizes. This entails leveraging very deep networks, enhanced by residual layers, and the strategic integration of dilated convolutions to enable the model to effectively examine a substantial portion of the past for making accurate predictions. TCN utilizes three main techniques: causal convolutions, dilated convolutions, and residual connections. Causal convolutions, a fundamental aspect of TCNs, ensure that the output at a given time step depends solely on the present or past inputs from the previous layer. This concept enhances the network's ability to capture temporal dependencies effectively. Zero-padding is strategically used in hidden layers to maintain consistent dimensionality with the input layer, facilitating seamless convolutions. Dilated convolutions represent another key feature of TCNs, introduced to address the challenge of capturing long-range dependencies. Unlike causal convolutions alone, which may require a very deep neural network, dilated convolutions enable larger receptive fields without an excessively deep architecture. The dilated convolutional operator operates on sequence elements, considering a defined filter, input sequence, filter size, and dilation factor. The dilation factor increases exponentially with the network's depth, creating a pyramidal structure that effectively expands the network's receptive field [41].

Residual connections, inspired by residual blocks, play a crucial role in overcoming the gradient vanishing problem often encountered in deep networks. By integrating shortcut connections in the form of residual blocks, TCNs allow the network to learn modifications to the identity mapping rather than the entire transformation. This mechanism contributes to more stable training and

facilitates the learning of complex relationships within the data. The architecture of a TCN includes a series of dilated causal convolutional layers within a residual block. However, challenges arise when the input and output of the residual block have different widths. To address this, a 1x1 convolutional layer is applied, ensuring consistent widths for the element-wise addition operation. This meticulous design enhances the network's ability to capture intricate patterns in sequential data. The advantages of TCNs are notable across various dimensions. Their larger receptive field size allows for the effective capture of long-range dependencies, providing a significant advantage in tasks requiring memory of past inputs. Stable gradients, a key characteristic of TCNs, are facilitated by a backpropagation path that differs from the temporal direction of the sequence. This feature mitigates the issues of exploding or vanishing gradients, which can be prominent concerns in recurrent architectures. Additionally, TCNs offer benefits in terms of parallelism, flexibility in receptive field size, stability of gradients, low memory requirements for training, and the ability to handle variable-length inputs. Unlike recurrent neural networks (RNNs), where predictions for later time steps are contingent on predecessors completing, TCNs enable parallel processing since the same filter is used in each layer. This parallelism accelerates both training and evaluation, allowing a long input sequence to be processed as a whole. The flexible receptive field size of TCNs is a notable advantage. By stacking more dilated (causal) convolutional layers, adjusting dilation factors, or increasing filter size, the model can adapt to different domains and memory requirements. This flexibility allows for better control over the model's memory size, catering to diverse application scenarios. Additionally, TCNs offer benefits in terms of parallelism, flexibility in receptive field size, stability of gradients, low memory requirements for training, and the ability to handle variable-length inputs. Unlike recurrent neural networks (RNNs), where predictions for later time steps are contingent on predecessors completing, TCNs enable parallel processing since the same filter is used in each layer. This parallelism accelerates both training and evaluation, allowing a long input sequence to be processed. The flexible receptive field size of TCNs is a notable advantage. By stacking more dilated (causal) convolutional layers, adjusting dilation factors, or increasing filter size, the model can adapt to different domains and memory requirements. This flexibility allows for better control over the model's memory size, catering to diverse application scenarios.

Stable gradients further distinguish TCNs from traditional recurrent architectures. The backpropagation path in TCNs differs from the temporal direction of the sequence, mitigating the

problem of exploding or vanishing gradients. This characteristic is crucial for training deep networks effectively, contributing to improved convergence and model performance. Another noteworthy advantage is the low memory requirement for training, especially in the case of long input sequences. While long short-term memory (LSTM) and gated recurrent units (GRUs) can consume substantial memory to store partial results for multiple cell gates, TCNs share filters across a layer, leading to lower memory usage. This efficiency is particularly beneficial in resource-intensive applications where memory constraints are a concern. Furthermore, TCNs demonstrate adaptability to variable-length inputs. Like RNNs, which model inputs with variable lengths recurrently, TCNs can process inputs of arbitrary lengths by sliding 1D convolutional kernels. This feature makes TCNs versatile and capable of serving as drop-in replacements for RNNs in scenarios involving sequential data of varying lengths.A deeper exploration of TCNs reveals their reliance on residual blocks containing two layers of dilated causal convolution and non-linear activation, typically implemented using the rectified linear unit (ReLU). For normalization, weight normalization is applied to convolutional filters and spatial dropout is incorporated after each dilated convolution for regularization. The combination of these techniques within a residual block contributes to the model's ability to learn complex patterns and adapt to different datasets. In summary, Temporal Convolutional Networks present a compelling solution

for sequence modeling tasks, leveraging causal convolutions, dilated convolutions, and residual connections to address key challenges associated with long-range dependencies, gradient stability, and memory efficiency. The architectural innovations within TCNs contribute to their superior performance in various applications, making them a promising choice for researchers and practitioners working on tasks involving sequential data analysis.
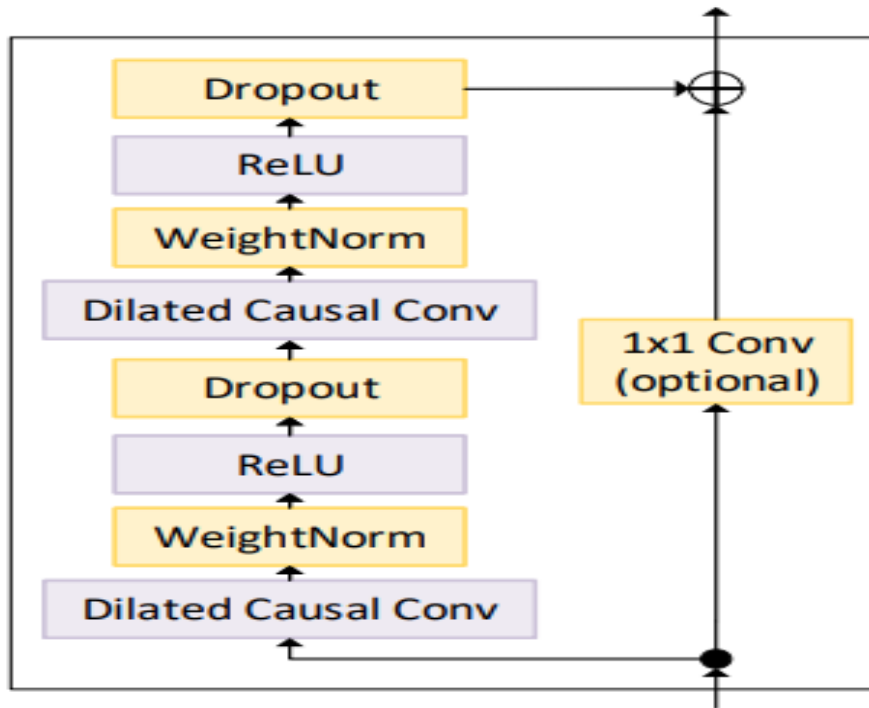
Figure 3.14 Residual block
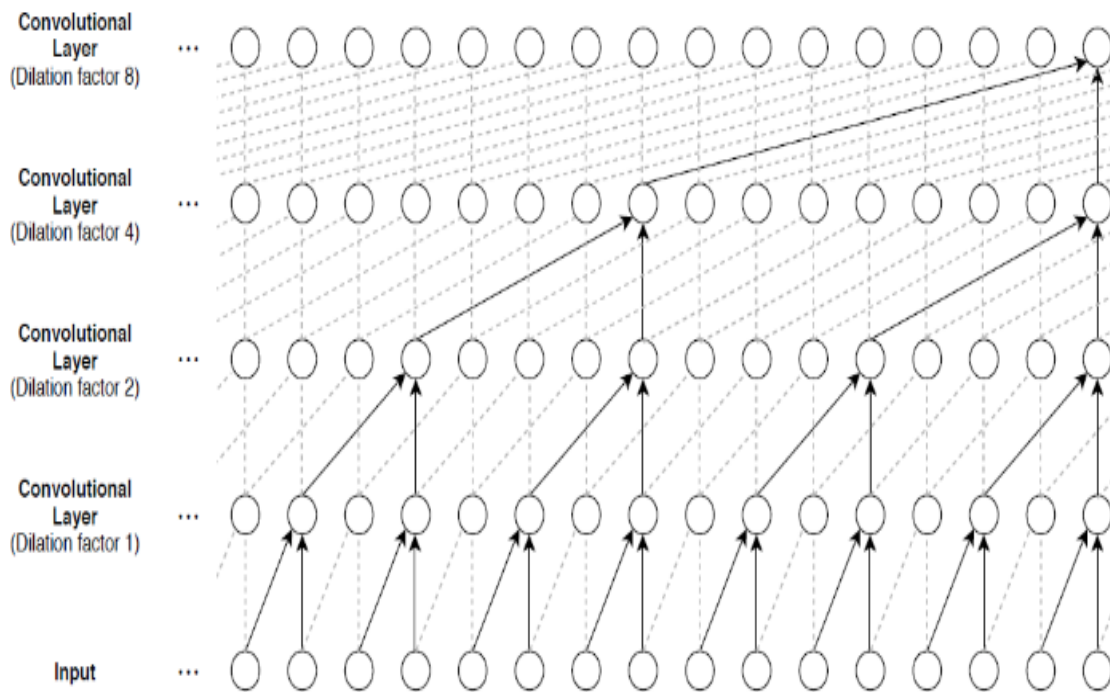
Figure 3.15 Architecture of TCN

3.5.2 Long Short-Term Memory

Long Short-Term Memory (LSTM) stands as a pivotal architecture within the realm of recurrent neural networks (RNNs), especially renowned for its prowess in capturing long-term dependencies—a quality that renders it particularly well-suited for sequence prediction tasks. In essence, LSTM has become a cornerstone in the landscape of deep learning, offering an effective solution for processing sequential data such as time series, text, and speech. Proposed by Hochreiter and Schmidhuber, LSTM revolutionized sequential data processing by offering a mechanism to retain information over extended periods. Unlike its predecessor, where predicting words stored in long-term memory proved challenging, LSTM excelled in providing more accurate predictions by effectively leveraging recent information. The inefficiency of RNNs in handling increased gap lengths further underscored the need for LSTM's intervention [42]. The genesis of LSTM can be traced back to the persistent challenge encountered by traditional RNNs—the vanishing error problem. This limitation prompted the development of LSTM as a gradient-based method specifically tailored to address the shortcomings associated with long-term dependencies in RNNs.

In contrast to conventional neural networks, LSTM introduces feedback connections, endowing it with the capability to process entire sequences of data rather than focusing on individual data points. This intrinsic feature empowers LSTM networks to discern and predict patterns embedded within sequential data, making them invaluable in diverse applications. The structural underpinning of LSTM comprises a chain-like arrangement housing four neural networks and specialized memory blocks known as cells. These cells play a crucial role in facilitating the handling of information over prolonged durations, a distinctive trait that sets LSTM apart. The following equation is on the Cell state operation of LSTM: $C_t = f_t * C_{t-1} + i_t * \breve{C}_t$

The Forget Gate represents an integral component of LSTM, acting as the mechanism for removing information that is deemed no longer useful in the cell state. It operates through the inputs at a particular time (x_t) and the previous cell output(h_{t-1}). The gate utilizes weight matrices and bias, followed by an activation function, to decide whether to forget or retain specific information. The forget gate's ability to selectively discard irrelevant information ensures the efficiency of LSTM in managing memory.

$$f_t = \sigma(W_f|h_{t-1}, x_t| + b_t$$
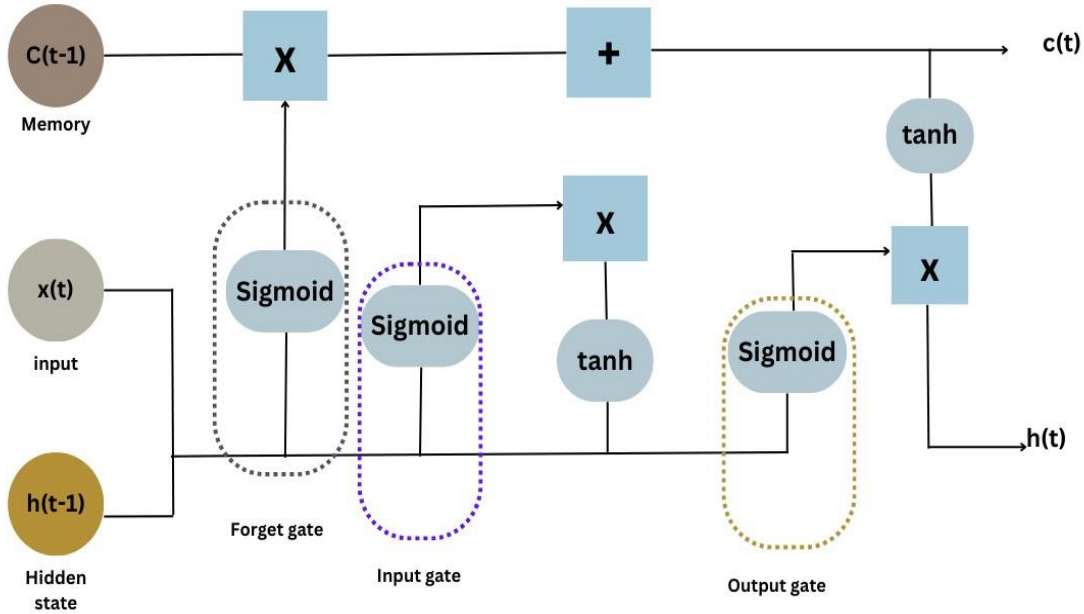
Figure 3.16 Architecture of LSTM

Where t=timestep, f_t=Forgot gate at t, b_f=connection bias at t, x_t=input, h_{t-1} =Previous hidden state, w_f=Weight matrix between forget gate and input gate

The Input Gate, another crucial element within the LSTM structure, plays a pivotal role in determining what information should be added to the memory cell. This gate operates through a series of computations involving inputs at a specific time (x_t) and the previous cell output (h_{t-1}). The weighted inputs, combined with bias, undergo an activation function, typically a sigmoid function. The sigmoid activation function squashes the output to a range between 0 and 1, effectively serving as a gating mechanism. If the output is close to 1, it indicates that the corresponding information is essential and should be retained in the memory cell. Conversely, if the output is closer to 0, it suggests that the information is less relevant and can be filtered out.

$$i_t = \sigma(W_i|h_{t-1}, x_t| + b_t$$

$$\breve{C}_t = \tanh(W_C * [h_{t-1}, x_t] + b_c$$

Where t=timestep, i_t=input gate at t, x_t=input, h_{t-1} =Previous hidden state , b_t=connection bias at t, b_t=connection bias at t w.r.t W_c, W_i=Weight matrix of sigmoid operator between input gate and output gate, W_c=Weight matrix of tanh operator between cell state information and network output

Conversely, the Output Gate plays a complementary role in LSTM, extracting valuable information from the current cell state for presentation as the output. The process involves generating a vector through the application of the hyperbolic tangent (tanh) function on the cell. This vector is then regulated using the sigmoid function, filtering the values to be remembered based on the inputs h_t-1 and x_t. The final step involves multiplying the vector with the regulated values, serving as both the output and input to the next cell. The output gate's meticulous regulation ensures that only pertinent information is disseminated, contributing to LSTM's ability to learn and remember complex patterns in sequential data.

$$o_t = \sigma(W_o|h_{t-1}, x_t| + b_o$$

$$h_t = o_t * \tanh(C_t)$$

Where t=timestep, o_t=output gate at t,, x_t=input, h_{t-1} =Previous hidden state, b_o= connection bias at t w.r.t W_o, W_o=Weight matrix of the output gate

The architecture of LSTM extends beyond its components, allowing for the stacking of multiple LSTMs to create deep LSTM networks. This stacking enhances the model's capacity to discern intricate patterns within sequential data, contributing to its versatility in handling complex datasets.

In the broader landscape of deep learning, LSTMs find compatibility with other neural network architectures, showcasing their adaptability. The fusion of LSTMs with Convolutional Neural Networks (CNNs) in image and video analysis exemplifies the model's flexibility and applicability across diverse domains. In conclusion, Long Short-Term Memory emerges as a robust and versatile architecture within the realm of recurrent neural networks. Its distinctive features, including causal convolutions and the ability to handle sequences of varying lengths, position it as a key player in sequence prediction tasks. The structural components, such as Forget Gates and

Output Gates, contribute to LSTM's efficacy in managing long-term dependencies and discerning complex patterns. The evolution of LSTM reflects a pivotal advancement in the field of deep learning, offering solutions to challenges encountered by traditional RNNs and proving instrumental in various applications, from natural language processing to time series forecasting.

3.5.3 Hybrid Architecture with Temporal Convolutional Networks (TCNs) and Long Short-Term Memory (LSTM) Networks

Combining Temporal Convolutional Networks (TCNs) and Long Short-Term Memory (LSTM) networks creates a powerful hybrid architecture for dealing with sequences of data. TCNs are great at quickly understanding short-term patterns in sequences, while LSTMs excel at grasping longer-term dependencies. This hybrid approach aims to get the best of both worlds, addressing the weaknesses of each model. TCNs work well in parallel, handling short-term patterns efficiently. They use convolutional layers to extract features from the input data. On the other hand, LSTMs are good at storing and learning from long-term dependencies in sequences. By combining TCNs and LSTMs, the hybrid model becomes capable of understanding both the immediate context and crucial historical information.

In this setup, TCNs often process the input sequence first, capturing short-term dependencies. LSTMs then come into play at later stages of the network, focusing on storing important long-term dependencies that may stretch across the entire input sequence. This way, the hybrid model maintains a balance between recognizing immediate patterns and retaining crucial historical information.

Practically, this hybrid architecture has shown promise in various applications. For example, in predicting time series data, the model can effectively capture short-term changes and long-term trends, leading to more accurate forecasts. Similarly, in natural language tasks, the hybrid approach proves useful in understanding both the immediate meaning of words and the overall structure of sentences. As we look to the future of deep learning, this blending of TCNs and LSTMs reflects a pragmatic approach to handling real-world data complexities. The hybrid architecture offers a flexible solution that combines the strengths of two effective models, providing a well-rounded approach to analyzing sequences of data. It not only pushes the boundaries of what deep learning

can achieve but also highlights the significance of integrating different methods to explore new possibilities in research and practical applications.

3.5.4 Artificial Neural Networks

3.5.1.1 <u>Medium Neural Networks:</u>

Medium neural networks strike a balance between the simplicity of narrow networks and the power of wider ones. The term "medium" refers to a moderate number of neurons, chosen intentionally to handle complexity while staying computationally efficient. These networks are versatile and work well for various tasks and datasets. With a moderate capacity, they capture intricate patterns without getting too complex and overfitting, a common problem in larger models. Medium networks have reasonable computational demands, making them suitable for datasets of different sizes. Their adaptability makes them practical for applications where finding a balance between efficiency, generalization, and modeling intricate data relationships is important. Just like any neural network, it's essential to fine-tune and experiment to tailor the model to specific task needs.
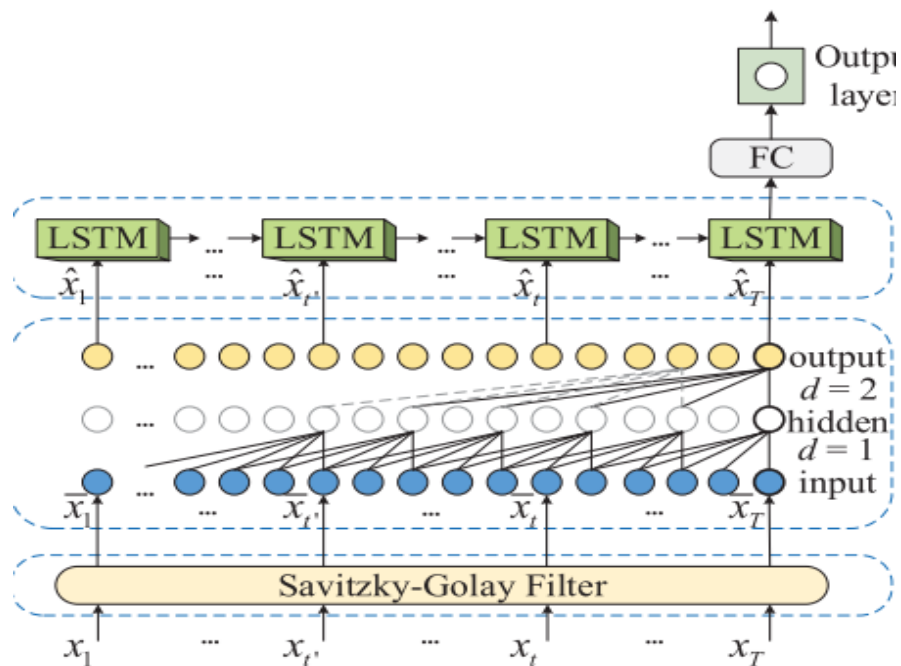
Figure 3.17 Hybrid Architecture with Temporal Convolutional Networks (TCNs) and Long Short-Term Memory (LSTM) Networks

3.5.1.2 Narrow Neural Networks:

Narrow neural networks, within the realm of artificial intelligence, denote architectures characterized by a more modest count of neurons in their hidden layers when compared to wider counterparts. The term "narrow" does not imply a limitation, but rather a conscious choice toward a more restrained complexity. These networks, with their fewer hidden layer neurons, offer distinct advantages in certain contexts. Computational efficiency emerges as a notable strength, as the training and inference processes are expedited due to the reduced number of parameters to compute and update. Moreover, narrow networks often exhibit enhanced generalization capabilities, particularly in scenarios where datasets are limited. Their propensity to avoid overfitting, a phenomenon where the model memorizes training data rather than learning patterns, is a valuable characteristic, contributing to improved performance on new, unseen data. This is particularly relevant in cases where simplicity and interpretability are priorities. The elegance of narrow networks lies in their ability to strike a balance, offering computational efficiency without compromising the model's capacity to discern intricate patterns within the data. Experimentation with various architectures, including different widths, remains a common practice to tailor the neural network to the unique demands of specific tasks and datasets.

3.5.1.3 Multilayer Perceptron (MLPs):

Multilayer Perceptron (MLPs) represent a fundamental and versatile class of artificial neural networks that have played a pivotal role in shaping the landscape of machine learning. Originating from the broader family of neural networks, MLPs have evolved into a cornerstone of deep learning, demonstrating exceptional prowess in various applications. In this comprehensive exploration, we delve into the intricacies of MLPs, unraveling their theoretical foundations, architectural components, training methodologies, and diverse real-world applications.

At its essence, an MLP is a feedforward neural network with three or more layers: an input layer, one or more hidden layers, and an output layer. The neurons, or nodes, within each layer, are interconnected, forming a network structure that allows information to flow in a unidirectional manner, from the input layer through the hidden layers to the output layer. The term "perceptron" reflects the basic unit of computation within these networks, inspired by the mathematical model of a biological neuron. The strength of MLPs lies in their capacity to learn complex patterns and

representations from data. Each connection between neurons is associated with a weight, and each neuron has an associated bias. During training, these weights and biases are adjusted through an iterative optimization process, commonly known as backpropagation, to minimize the difference between the predicted and actual outputs. The non-linear activation functions applied to each neuron introduce non-linearity into the model, enabling MLPs to capture intricate relationships within the data.

The hidden layers of an MLP contribute to its ability to learn hierarchical representations. As data passes through successive hidden layers, the network can extract progressively abstract features. This hierarchical feature learning is crucial for tasks such as image recognition, where lower layers may capture basic shapes, and higher layers combine these shapes to recognize more complex patterns. A defining feature of MLPs is their universal approximation theorem, which states that a feedforward neural network with a single hidden layer containing a finite number of neurons can approximate any continuous function on a closed and bounded input space to arbitrary accuracy. This theorem underscores the expressive power of MLPs, making them capable of approximating highly complex and non-linear mappings between inputs and outputs. Training an MLP involves presenting the network with a set of input-output pairs, known as the training dataset, and adjusting the weights and biases to minimize the error between the predicted and actual outputs. The backpropagation algorithm, coupled with optimization techniques like stochastic gradient descent, facilitates this weight adjustment process. Regularization techniques, such as dropout and weight decay, are often employed to prevent overfitting and enhance generalization to unseen data.

The architecture of MLPs can vary widely based on the specific task and dataset. Common variants include deep MLPs with multiple hidden layers, wide MLPs with a large number of neurons in each layer, and specialized architectures like convolutional neural networks (CNNs) for image data and recurrent neural networks (RNNs) for sequential data.

3.5.1.4 Backpropagation Neural Networks:

Backpropagation Neural Networks leverage the backpropagation algorithm for training, marking a significant advancement in the field of neural networks. The backpropagation algorithm allows networks to iteratively adjust their weights based on the error between predicted and actual outputs. This optimization process enables the efficient learning of intricate patterns in diverse datasets.

Backpropagation networks are often implemented with multiple layers, contributing to the emergence of deep learning architectures. These networks have played a pivotal role in the success of neural networks, overcoming challenges associated with vanishing and exploding gradients. The ability to efficiently train deep networks has led to breakthroughs in various domains, including computer vision, natural language processing, and speech recognition. While the training of deep networks can be computationally intensive, the benefits in terms of improved performance and feature representation have fueled their widespread adoption in modern machine learning applications.

3.5.1.5 <u>Cubic Support Vector Machine</u>

Support Vector Machine (SVM) analysis stands as a cornerstone in the realm of machine learning, with its roots tracing back to 1992 when Vladimir Vapnik and his colleagues introduced this powerful tool for classification and regression. The SVM approach revolutionized the field, offering a robust framework for solving complex problems in various domains. In this exploration, we delve into the intricacies of SVM regression, a nonparametric technique that hinges on the ingenious use of kernel functions to unearth patterns and relationships within data.

SVM regression is fundamentally distinct from its classification counterpart but inherits the core principles that make SVM a stalwart in the machine learning landscape. While SVM classification carves decision boundaries to segregate data into distinct classes, SVM regression takes a different path, aiming to predict continuous outcomes. It does so by fitting a hyperplane in a high-dimensional space defined by the chosen kernel function, seeking optimal generalization performance. The primary concept driving SVM regression is the identification and minimization of residuals, the differences between predicted and actual values. This is achieved by defining a tube, often cubic in nature, of a specified width (ϵ-sensitivity). The algorithm then selectively considers residuals falling within this tube, effectively prioritizing those that align closely with the predicted function. Points inside the tube are considered ϵ-close and are not penalized, fostering a nuanced approach to handling deviations from the expected outcome.

Conversely, points lying outside the tube are penalized based on their distance from the predicted function. This penalization mechanism ensures that the algorithm not only captures the general trend within the data but also accounts for variations that fall outside the designated tolerance. This

bears a resemblance to the penalization strategy employed by SVMs in classification, underlining the unified nature of SVM principles across different problem domains. The elegance of SVM regression lies in its ability to strike a balance between capturing essential patterns within the data and mitigating the impact of outliers or noise. By focusing on residuals within the defined tube, the model aims to achieve a robust fit that generalizes well to unseen data. This approach to regression aligns with the broader philosophy of SVM, emphasizing structural risk minimization and the pursuit of a solution that maintains a favorable bias-variance trade-off.

The broader context of SVM regression, as an extension of the SVM framework, also brings forth considerations related to kernel functions. These functions play a pivotal role in SVM by transforming the input data into a higher-dimensional space, where the underlying patterns become more apparent. The choice of kernel function significantly influences the model's ability to capture complex relationships, and popular choices include radial basis functions (RBF), polynomial kernels, and, in the case of cubic SVM, cubic kernels. The cubic SVM, with its emphasis on a cubic tube for handling residuals, aligns with the overarching objective of SVM regression—to find a well-fitting hyperplane in a kernel-induced feature space. This hyperplane encapsulates the essential relationships within the data, and the cubic nature of the tube provides the model with the capacity to navigate non-linearities inherent in the data distribution.

While the detailed theoretical underpinnings of Support Vector Regression (SVR) are not explicitly covered in this exploration, it is essential to acknowledge the wealth of knowledge available in seminal works such as Burges (1998) and references like Awad and Khanna. These sources offer in-depth insights into SVR theory, providing a comprehensive understanding of the mathematical foundations and principles that govern the successful application of SVM regression. The cubic kernel function, a key feature of Cubic SVMs, introduces a cubic transformation to the input data. This transformation enables the model to capture complex patterns and non-linear relationships that may exist in the data. Mathematically, the cubic kernel function is defined as

$$k(x, y) = ((x * y) + c)^3$$

, where 'c' is a constant term.

3.6 Evaluation metrics

The models will be evaluated using 4 evaluation metric i-e mean square error (MSE), root mean square error (RMSE), mean absolute error (MAE) and coefficient of determination (R^2).

3.6..1   Mean absolute error.

Mean absolute error is key metric for evaluating the performance of a regression model. he term "error" denotes the difference between the actual force values and the corresponding predictions made by the model. To quantify these differences, the absolute function is employed, ensuring that all disparities are considered in a positive light.

Mathematically, the Absolute function transforms any negative values to their positive counterparts, capturing the magnitude of the error. The MAE is then computed by determining the average of these absolute error values. Crucially, the units associated with MAE remain consistent with those of the true and predicted force, maintaining uniformity in the measurement scale (e.g., Newton, N).

In our context, where force is the focal parameter, MAE encapsulates the average magnitude of the disparities between predicted and actual force values. Therefore, a lower MAE indicates a more accurate model, suggesting that, on average, the predictions closely align with the true force measurements. The mathematical formula of Mean absolute error is:

$$MAE = \frac{\sum_{i=1}^{n} |y_i - x_i|}{n}$$

3.6..2   Mean Square Error

Mean Squared Error (MSE) is a crucial metric for evaluating the performance of regression models. It quantifies the average of the squared differences between observed and predicted values. The mathematical formulation for MSE involves squaring each individual error, emphasizing the significance of larger errors in the overall assessment of model accuracy.

$$MSE = \frac{1}{n}\sum_{i=1}^{n}(x_i - y_i)^2$$

This mathematical metric emphasizes larger errors, assigning them greater weight in the assessment of model performance. When a model is perfectly accurate, MSE equals zero, but as errors increase, so does its value. MSE is synonymous with Mean Squared Deviation (MSD), highlighting its role in quantifying the deviation or discrepancy between observed and predicted values. The units of MSE are the square of the original units of the observed and predicted values, such as square Newtons (N^2) if the variable of interest is force in Newtons. While sensitive to outliers due to the squaring of errors, MSE provides a comprehensive measure, aiding in the nuanced evaluation of regression models based on the nature of the dataset and the desired emphasis on different types of errors.

3.6..3 Root Mean Square Error

Root Mean Squared Error (RMSE) is a pivotal metric for assessing the predictive accuracy of a statistical model, capturing the average difference between the model's predicted values and the actual observed values.

$$RMSE = \sqrt{\frac{\sum_i^n (x_i - y_i)^2}{n}}$$

Mathematically, RMSE corresponds to the standard deviation of the residuals, where residuals denote the vertical distance between individual data points and the regression line. In essence, RMSE serves as a comprehensive measure by quantifying the dispersion of these residuals. It provides insight into how closely the observed data points cluster around the predicted values, offering a holistic view of the model's precision. As a root mean square, RMSE accounts for both the magnitude and direction of errors, making it a valuable tool for evaluating the overall performance and predictive power of regression models across a dataset.

3.6..4 Coefficient of Determination (R^2)

The coefficient of determination, commonly known as R^2, is a crucial metric in regression analysis that evaluates the proportion of the variance in the dependent variable that is explained by the independent variables. Specifically, R^2 measures the goodness of fit of a regression model.

$$R^2 = 1 - \frac{\sum_{i=1}^{n}(x_i - y_i)^2}{\sum_{i=1}^{n}(x_i - y_i)^2}$$

It is calculated as the ratio of the explained variance to the total variance in the data. A higher R^2 value, closer to 1, indicates that a larger proportion of the variability in the dependent variable is accounted for by the model, suggesting a better fit. Conversely, a lower R^2 value, closer to 0, suggests that the model is less effective in explaining the variability. It's important to note that R^2 does not indicate the correctness of the model's coefficients but rather the adequacy of the model in capturing the variance in the data. While R^2 is a valuable metric, it should be used in conjunction with other evaluation measures to provide a comprehensive assessment of the model's performance.

3.7 Statistical Analysis

The evaluation of all model performances will be conducted using analysis of variance (ANOVA) to systematically assess which model demonstrates superior performance and whether there exists a statistically significant difference among them. This rigorous statistical approach will provide valuable insights into the effectiveness of each model in predicting force, helping identify the most reliable and accurate one. Furthermore, a comparative analysis of results will be undertaken for force prediction based on surface electromyography (SEMG) and integrated electromyography (IEMG). This investigation aims to unveil any significant disparities between the predictive capabilities of these two methodologies. Additionally, a comparative examination of model outcomes between healthy individuals and amputees will be conducted, shedding light on potential distinctions in predictive accuracy for these diverse user groups. Through this comprehensive analysis, the study seeks to discern not only the optimal model for force prediction but also potential variations in performance across different prediction methodologies and user demographics.

CHAPTER 4: RESULTS

4.1 Abled bodies

Following the stages of filtration and segmentation, the process proceeded to feature extraction for the machine learning models. The extracted features were then utilized as inputs for these models. Conversely, for the deep learning model, the segmented and filtered data itself served as the input. In the case of able-bodied individuals, eight distinct force patterns were identified, with two force profiles recorded for each. This detailed approach in handling the data ensures a robust foundation for both machine learning and deep learning models, contributing to a comprehensive analysis of force patterns in able-bodied subjects.

4.1.1   Temporal Convolutional network

The Temporal Convolutional Network (TCN) exhibited remarkable performance in predicting force using both surface electromyography (sEMG) and integrated electromyography (iEMG) signals. The R^2 values demonstrated exceptional accuracy, ranging from 0.95 to 0.97 for sEMG-based predictions and 0.93 to 0.95 for iEMG-based predictions. These high R^2 values signify a strong correlation between the predicted and actual force values, highlighting the precision and reliability of the TCN model. Additionally, the models showcased minimal error values, with all error-related metrics consistently remaining below 0.5N. This exceptional accuracy and low error rate underscore the effectiveness of TCN in capturing and leveraging the temporal dynamics within the signals for robust force prediction.
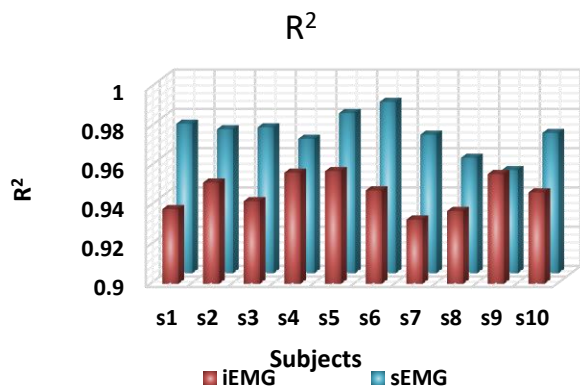
Figure 4.1 R^2 of TCN-based force prediction using sEMG and iEMG signals in able-bodied individuals.
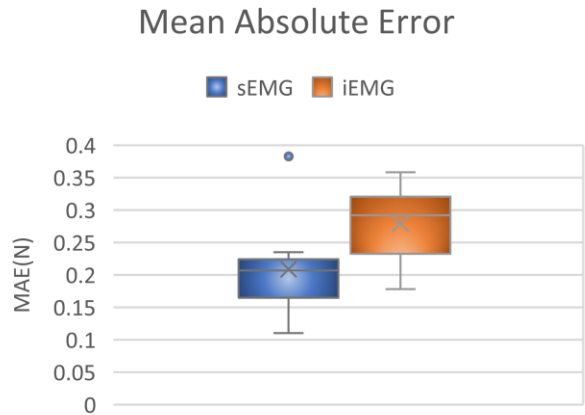
Figure 4.2 MAE of TCN-based force prediction using sEMG and iEMG signals in able-bodied individuals
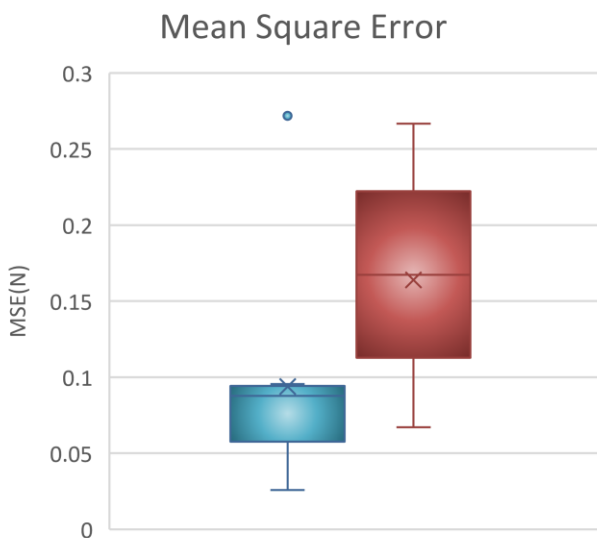
Figure 4.3 MSE of TCN-based force prediction
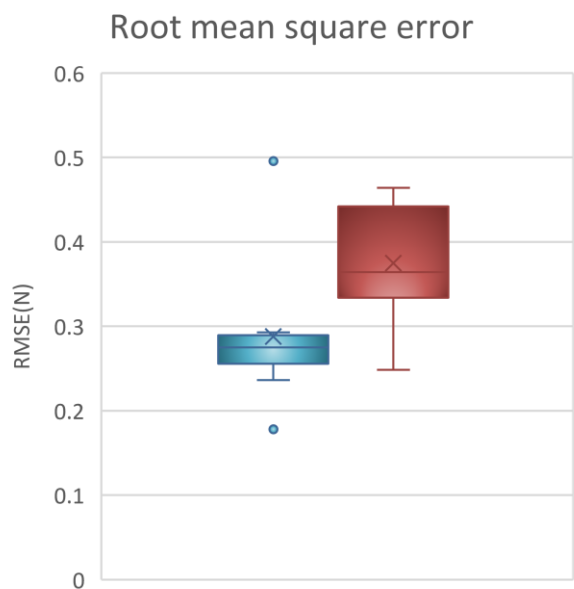
Figure 4.4 RMSE of TCN-based force prediction

In Figure 25-27, the performance of TCN stands out prominently, exhibiting exceptional results with a higher R^2 value and lower error. Although there is a noticeable decrease in prediction accuracy when compared to surface EMG, the R^2 values still range impressively from 0.9 to 0.95. Additionally, the error values, while slightly increased, consistently remain below 1. This

underscores the robust performance of TCN in comparison to surface EMG, emphasizing its efficacy in achieving accurate predictions with minimal error.

4.1.2   *Hybrid Architecture with Temporal Convolutional Networks (TCNs) and Long Short-Term Memory (LSTM) Network*

The hybrid architecture, combining Temporal Convolutional Networks (TCN) and Long Short-Term Memory (LSTM), demonstrated remarkable performance in predicting force based on both surface electromyography (sEMG) and intramuscular electromyography (iEMG) signals in able-bodied individuals. Figures 4.5 to 4.8 illustrate the trends of key metrics, including R2 (coefficient of determination), RMSE (Root Mean Square Error), MAE (Mean Absolute Error), and MSE (Mean Squared Error).

For sEMG-based force prediction, the coefficient of determination (R^2) exhibited a high range from 0.9988 to 0.92235. This indicates a strong correlation between the predicted and actual force values. Additionally, MSE, MAE, and RMSE values showed consistent performance, ranging between 0.7 and 0.0024. These low values signify accurate predictions with minimal errors.

Similarly, in the case of iEMG-based force prediction, the hybrid architecture displayed excellent results. The R^2 ranged from 0.995 to 0.91, emphasizing the model's ability to capture the underlying patterns in the data. The MSE, MAE, and RMSE values in iEMG also demonstrated reliable performance, falling within the range of 1.07 to 0.01. These metrics collectively indicate the effectiveness of the hybrid TCN and LSTM architecture in accurately predicting force from iEMG signals.

In summary, the hybrid model consistently performed well across both sEMG and iEMG, as evidenced by high R^2 values and low MSE, MAE, and RMSE values. This suggests its potential for robust and precise force prediction, making it a promising approach in the field of electromyography-based applications for able-bodied individuals.
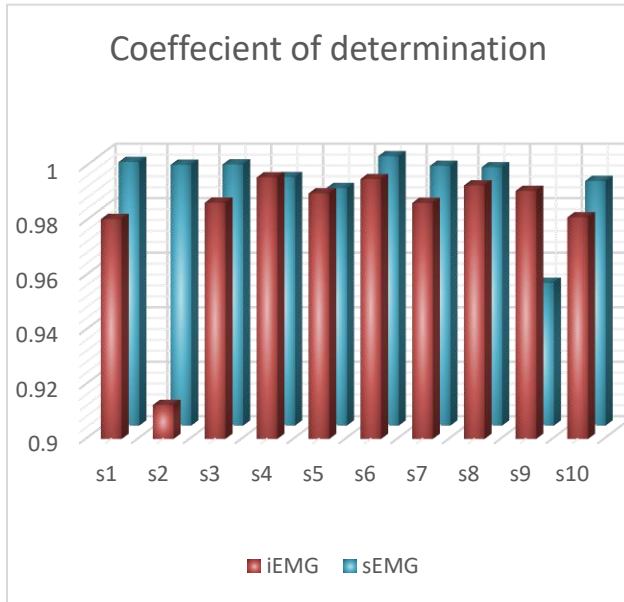
Figure 4.5 R^2 of TCN_LSTM-based force prediction

Figure 4.6 MAE of TCN_LSTM-based force prediction
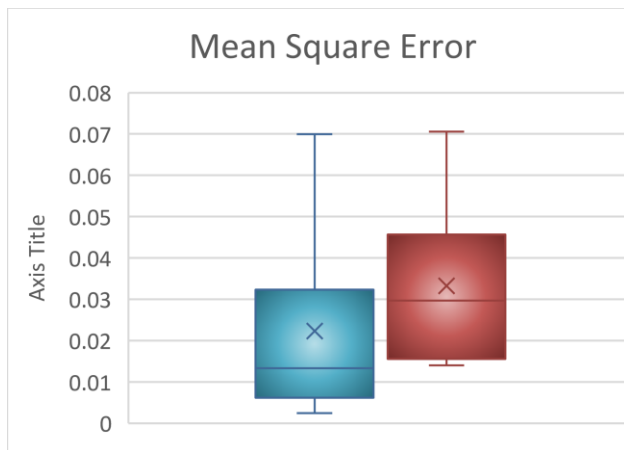
Figure 4.7 MSE of TCN_LSTM-based force prediction
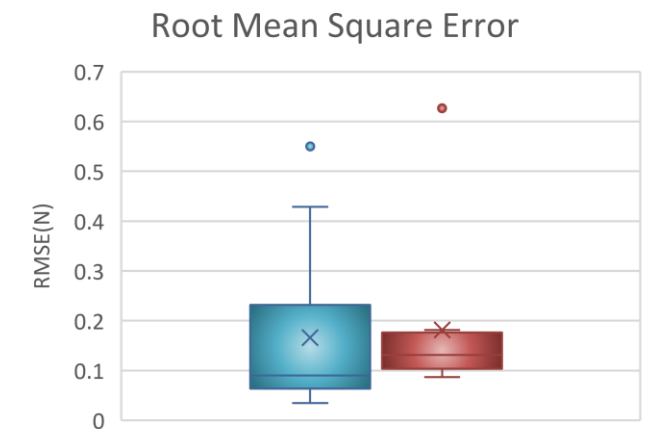
Figure 4.8 RMSE of TCN_LSTM-based force prediction

4.1.3 /Long Short-Term Memory

Long Short-Term Memory (LSTM) architecture showcased remarkable efficacy in predicting force based on both intramuscular electromyography (iEMG) and surface electromyography (sEMG) signals in individuals with normal physical abilities. Figures 4.9 to 4.12 visually depict the performance trends, highlighting key metrics such as R^2 (coefficient of determination), RMSE

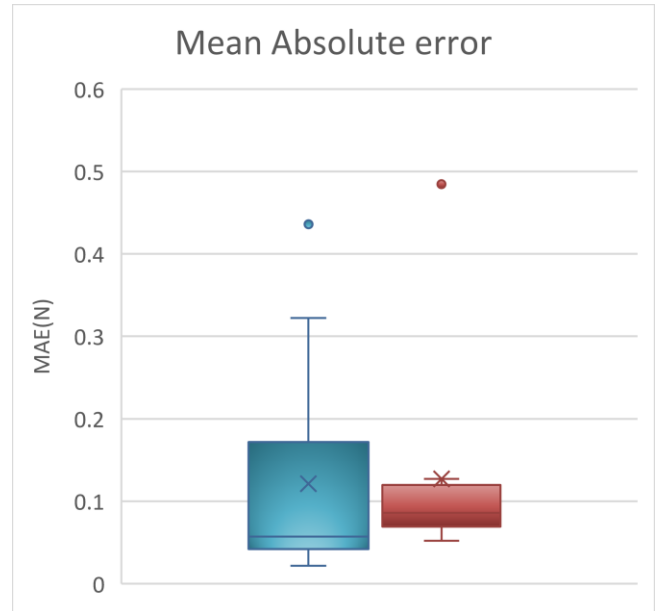(Root Mean Square Error), MAE (Mean Absolute Error), and MSE (Mean Squared Error). he LSTM model, when applied to surface electromyography (sEMG)-based force prediction, exhibited exceptional performance, as indicated by various evaluation metrics. The Mean Absolute Error (MAE) values ranged from 0.03 to 0.09, underscoring the model's ability to make highly accurate predictions with minimal deviation from the true values. Mean Squared Error (MSE) values spanned from 0.00 to 0.03, further highlighting the precision of the LSTM model in capturing the intricacies of the sEMG data. Root Mean Square Error (RMSE) values for sEMG prediction demonstrated a consistent range between 0.04 and 0.14. The coefficient of determination (R^2) values for sEMG predictions were consistently high, ranging from 0.97 to 1.00. This signifies an exceptionally strong correlation between the predicted and actual force values derived from sEMG signals.

Moving on to intramuscular electromyography (iEMG) results, the LSTM model continued to showcase outstanding predictive accuracy. For iEMG-based force prediction, the MAE ranged from 0.03 to 0.09, and MSE values spanned from 0.00 to 0.03, emphasizing the model's ability to make accurate predictions. The RMSE values for iEMG prediction demonstrated a narrow range, varying between 0.04 and 0.14, indicating consistent and accurate predictions. The coefficient of determination (R^2) for iEMG predictions was notably high, ranging from 0.97 to 1.00. This suggests an exceptionally strong correlation between the predicted and actual force values derived from iEMG signals.

In summary, the LSTM model consistently demonstrated exceptional predictive accuracy for both sEMG and iEMG-based force predictions. The low values of MAE, MSE, and RMSE, coupled with high R^2 values, underscore the robustness of the LSTM model in capturing and predicting force dynamics accurately from electromyography signals.

4.1.4 Gaussian process regression

4.1.4.1 Matern 5/2 kernel

The Gaussian Process Regression model proved to be a robust and effective approach for predicting force based on surface electromyography (sEMG) signals. Analyzing the results from Figures 4.13 to 4.16, the model demonstrated its capabilities with compelling metrics. The Mean

Absolute Error (MAE) for sEMG-based force prediction ranged from 0.13 to 0.45, showcasing the model's accuracy in minimizing deviations from actual force values. Correspondingly, the Mean Squared Error (MSE) varied between 0.03 and 0.41, and the Root Mean Square Error (RMSE) showed a range from 0.18 to 0.63, emphasizing the precision of the predictions. The Coefficient of Determination (R^2) values for sEMG predictions were noteworthy, ranging from 0.89 to 0.96.
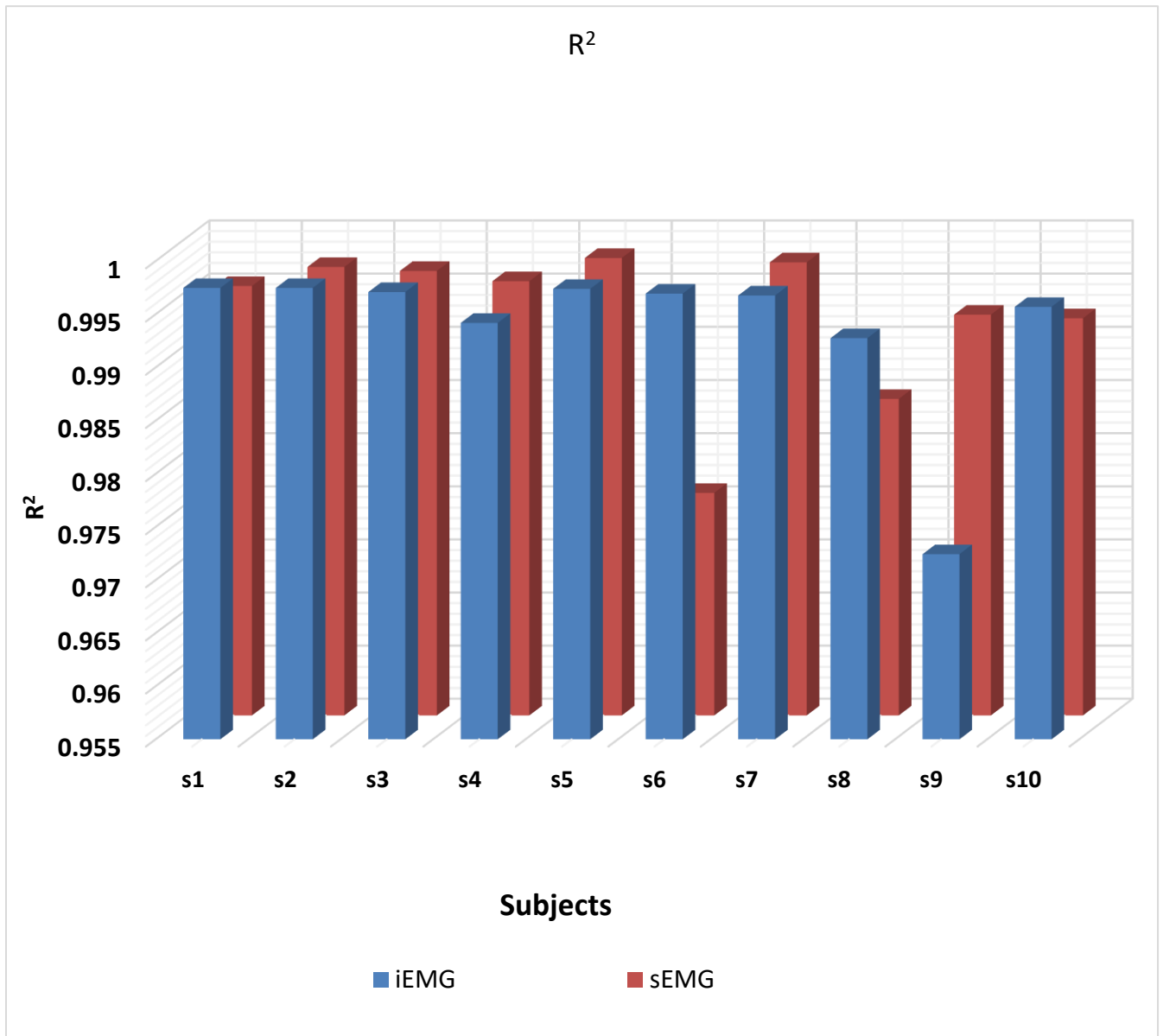
Figure 4.9 R^2 determination of LSTM-based force prediction

Mean Absolute Error
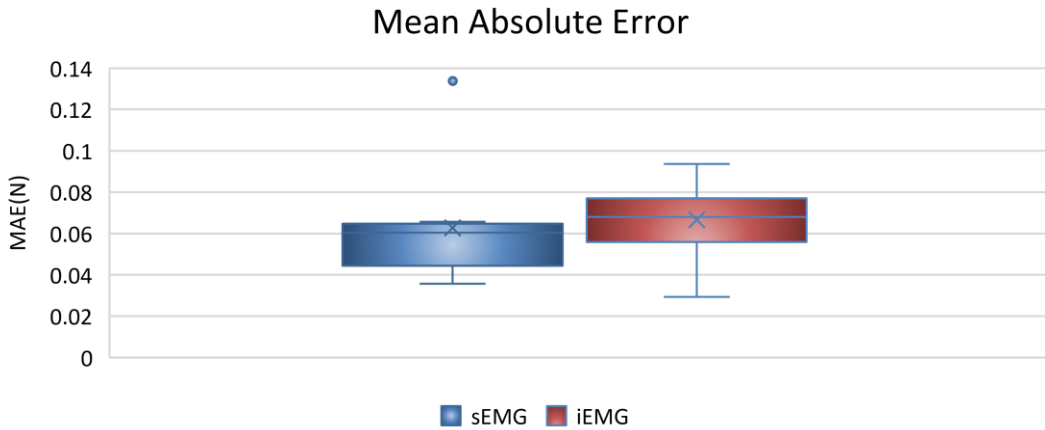
Figure 4.10 MAE of LSTM-based force prediction

Mean Square Error

Root Mean Square Error
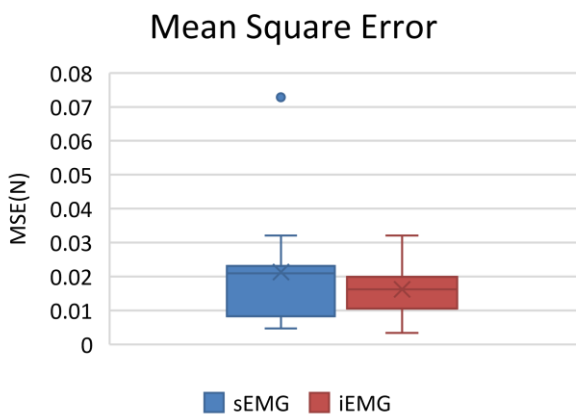
Figure 4.11 MSE of LSTM-based force prediction
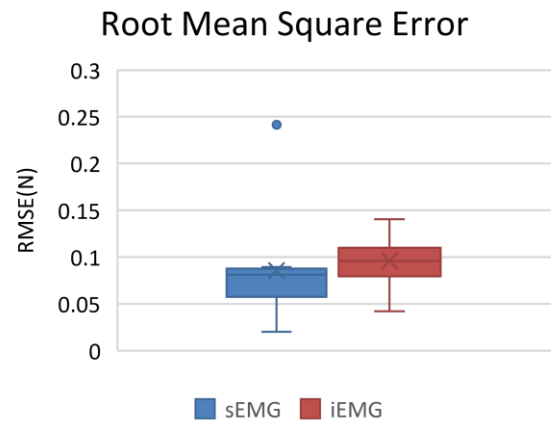
Figure 4.12 RMSE of LSTM-based force prediction

Turning to intramuscular electromyography (iEMG) predictions, the Gaussian Process Regression model continued to showcase its effectiveness. The MAE for iEMG-based force prediction ranged from 0.23 to 0.58, demonstrating accurate predictions with minimal deviations. The MSE values varied between 0.13 and 0.64, and the RMSE values showed a consistent range from 0.35 to 0.79, highlighting the model's reliability. The R^2 values for iEMG predictions were also notable, ranging from 0.86 to 0.92. These high R^2 values indicated a strong correlation between the predicted and actual force values derived from iEMG signals.In summary, Gaussian Process Regression

exhibited a robust performance for both sEMG and iEMG-based force predictions, as reflected in the presented metrics. The low MAE, MSE, and RMSE values, coupled with high R^2 values, underscore the model's accuracy and precision in capturing the dynamics of force prediction from electromyography signals.
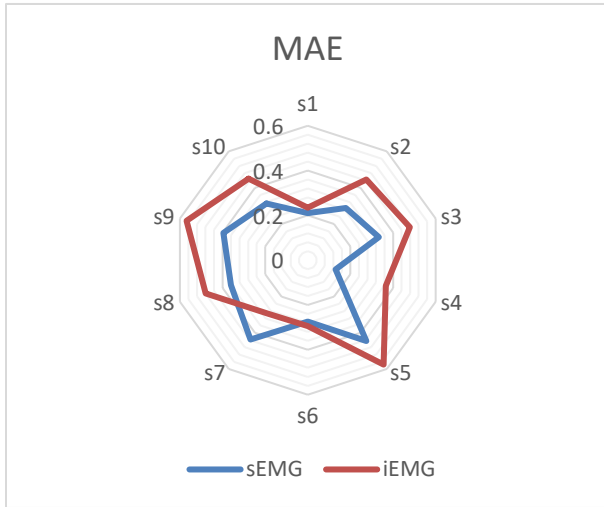
Figure 4.13 MAE of GPR (mat)-based force prediction
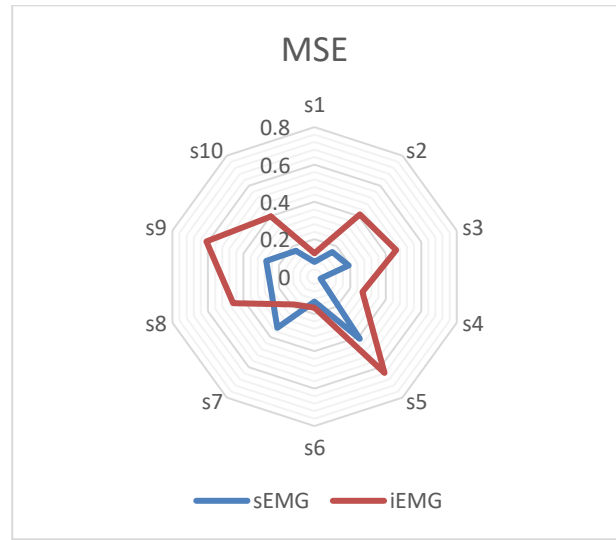
Figure 4.14 MSE of GPR (mat)-based force prediction
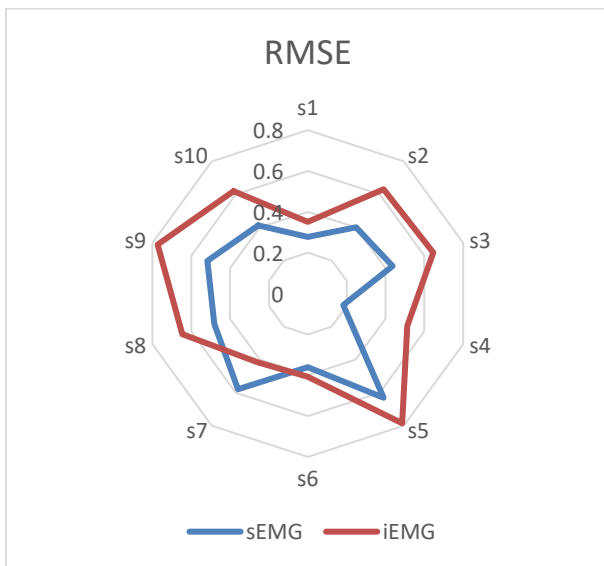
Figure 4.15 RMSE of GPR (mat)-based force prediction
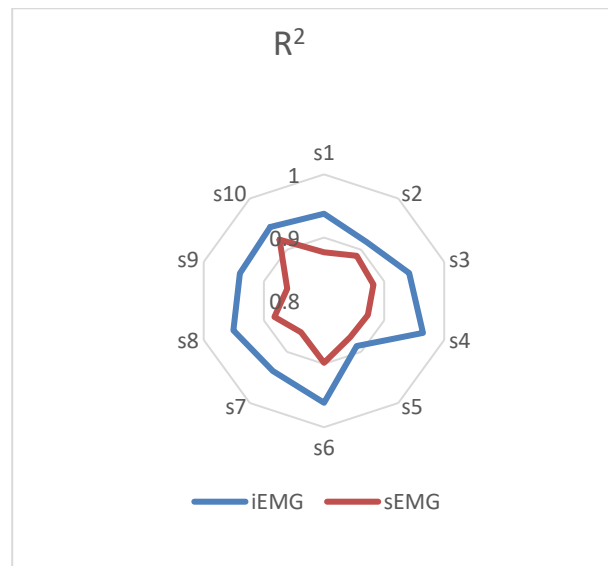
Figure 4.16 R^2 of GPR (mat)-based force prediction

4.1.4.2   Exponential kernel

Employing Gaussian Process Regression with an Exponential Kernel for surface electromyography (sEMG)-based force prediction yielded compelling results, as illustrated in Figures 4.17 to 4.19. The model exhibited noteworthy performance metrics, showcasing its ability to accurately predict force dynamics. The Mean Absolute Error (MAE) for sEMG predictions ranged from 0.14 to 0.45, indicating minimal deviation from actual force values. The Mean Squared Error (MSE) values varied between 0.04 and 0.39, underscoring the model's precision in capturing the intricacies of the sEMG data. The Root Mean Square Error (RMSE) values showed a consistent range from 0.19 to 0.61, further highlighting the accuracy of the model's predictions. The Coefficient of Determination (R^2) values for sEMG predictions using the Exponential Kernel ranged from 0.89 to 0.96. These high R^2 values affirm a strong correlation between the predicted and actual force values derived from sEMG signals, indicating the effectiveness of the Gaussian Process Regression model with an Exponential Kernel.

Turning to intramuscular electromyography (iEMG) predictions, the model continued to exhibit robust performance. The MAE for iEMG-based force prediction ranged from 0.24 to 0.58, showcasing accurate predictions with minimal deviations. The MSE values varied between 0.15 and 0.66, while the RMSE values consistently ranged from 0.38 to 0.80, emphasizing the reliability of the model's predictions. The R^2 values for iEMG predictions using the Exponential Kernel were notable, ranging from 0.86 to 0.92. These high R^2 values indicate a strong correlation between the predicted and actual force values derived from iEMG signals, highlighting the effectiveness of the Gaussian Process Regression model with an Exponential Kernel.

In summary, Gaussian Process Regression with an Exponential Kernel demonstrated robust performance for both sEMG and iEMG-based force predictions. The low MAE, MSE, and RMSE values, coupled with high R^2 values, underscore the model's accuracy and precision in capturing force dynamics from electromyography signals.
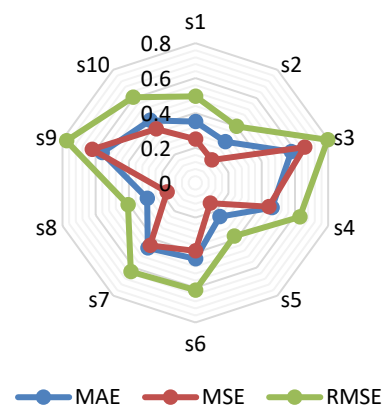
R²
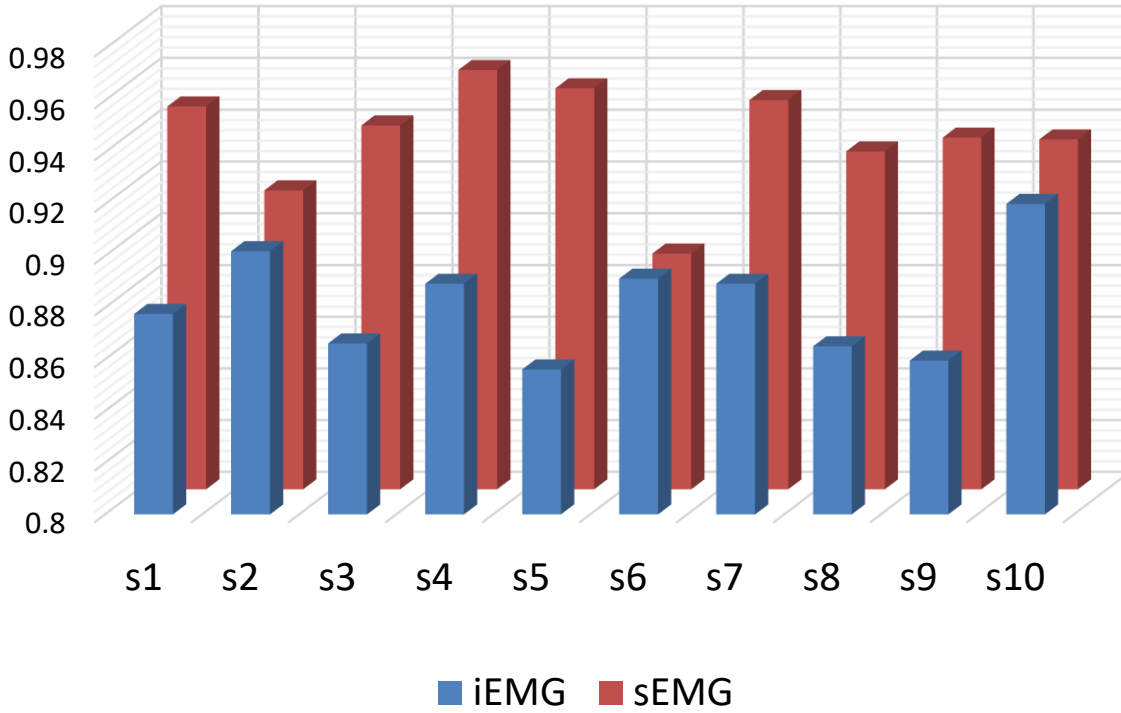
Figure 4.17 R^2 of GPR (EXPO)-based force prediction using sEMG and iEMG signals

Figure 4.18 Performance Metrics for GPR (expo) in sEMG-Based Force Prediction

Figure 4.19 Performance Metrics for GPR (expo) in iEMG-Based Force Prediction

4.1.5   Multilayer Perceptron

Utilizing Multilayer Perceptron (MLP) for force prediction based on surface electromyography (sEMG) signals yielded promising results, as demonstrated in Figures 4.20 and 4.21. The model showcased its predictive capabilities with compelling performance metrics. The Mean Absolute Error (MAE) for sEMG-based force prediction ranged from 0.15 to 0.49, indicating the model's ability to provide accurate predictions with minimal deviation from the actual force values. The Mean Squared Error (MSE) values varied between 0.04 and 0.51, while the Root Mean Square Error (RMSE) values consistently ranged from 0.21 to 0.71, highlighting the precision of the model's predictions. The Coefficient of Determination (R^2) values for sEMG predictions with MLP ranged from 0.87 to 0.96, indicating a strong correlation between the predicted and actual force values derived from sEMG signals. This emphasizes the effectiveness of the MLP model in capturing the underlying patterns in sEMG data for force prediction.

Similarly, for intramuscular electromyography (iEMG) predictions, the MLP model demonstrated reliable performance. The MAE for iEMG-based force prediction ranged from 0.26 to 0.69, indicating accurate predictions with minimal deviations. The MSE values varied between 0.17 and 0.97, while the RMSE values consistently ranged from 0.3 to 0.83, showcasing the model's precision in predicting force dynamics based on iEMG signals. The Coefficient of Determination (R^2) values for iEMG predictions with MLP ranged from 0.82 to 0.90, signifying a strong correlation between the predicted and actual force values derived from iEMG signals. This underscores the effectiveness of the MLP model in accurately capturing force dynamics from intramuscular electromyography.

Figure 4.20 Performance Metrics for MLP in sEMG-Based Force Prediction

Figure 4.21 Performance Metrics for in iEMG-Based Force Prediction

47

4.1.6   Medium Neural Network

The implementation of a Medium Neural Network for force prediction, utilizing surface electromyography (sEMG) and intramuscular electromyography (iEMG) signals, is outlined in Figures 4.22-4.24. The model's performance is characterized by key evaluation metrics, illustrating its capacity for accurate force predictions. The Medium Neural Network employed for force prediction based on surface electromyography (sEMG) and intramuscular electromyography (iEMG) signals has demonstrated varied effectiveness, as indicated by key evaluation metrics. However, the minimum values of the Coefficient of Determination (R^2), specifically 0.5 for sEMG and 0.44 for iEMG predictions, suggest limitations in the model's ability to explain the variability in the actual force values. These relatively lower R^2 values signify that a substantial portion of the force dynamics remains unaccounted for by the Medium Neural Network, indicating potential shortcomings in capturing the complex relationship between electromyography signals and force.

The observed lower R^2 values may stem from several factors, including the complexity of the underlying physiological processes, the need for a more sophisticated model architecture, or the presence of noise and variability in the data. These findings imply that the current model may not be as effective in accurately predicting force based on electromyography signals compared to other approaches.
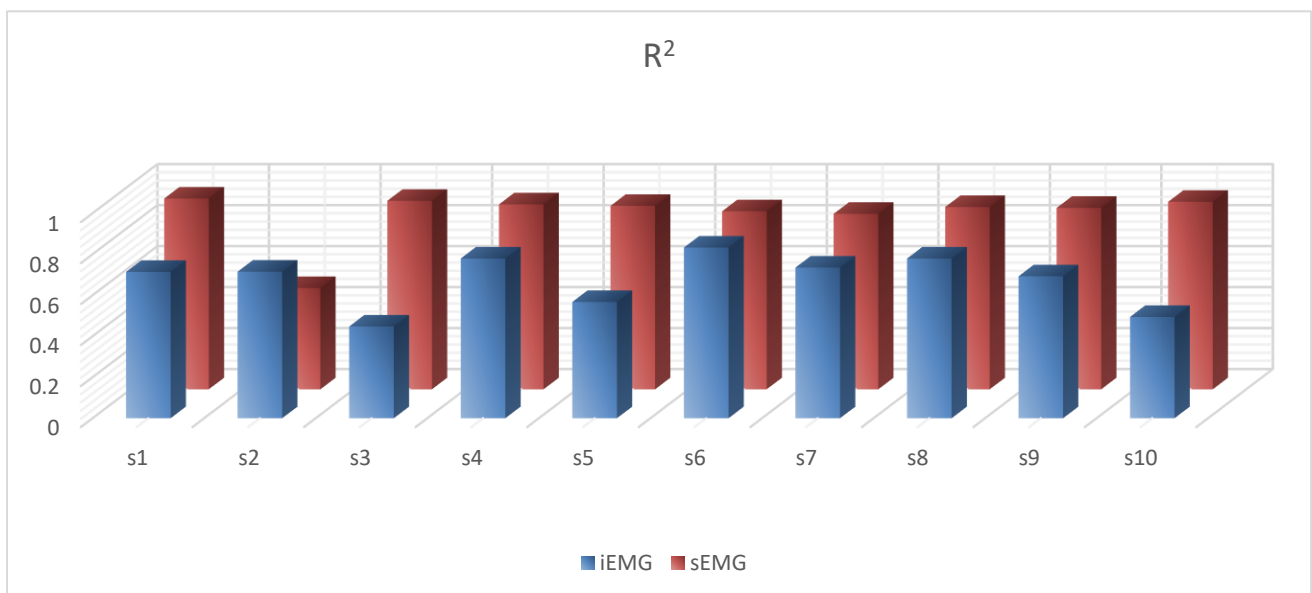
Figure 4.22 R^2 of MNN based force prediction using sEMG and iEMG signals.

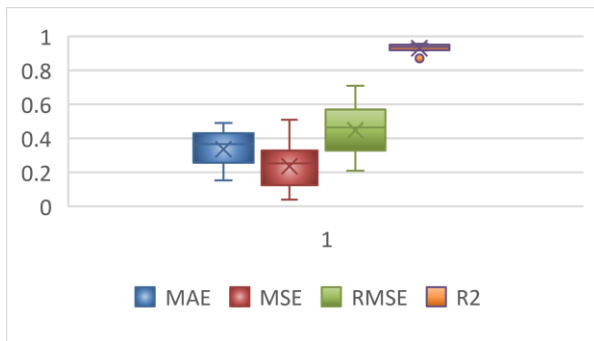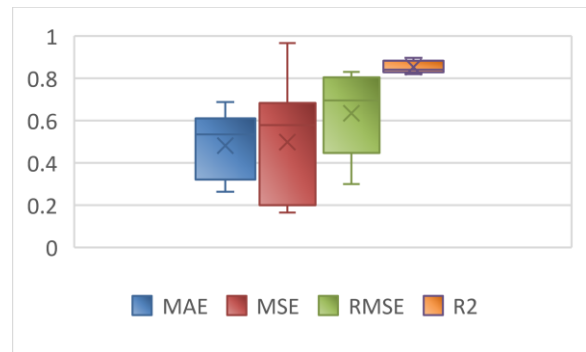**Figure 4.23** Performance Metrics for MNN in sEMG-Based Force Prediction

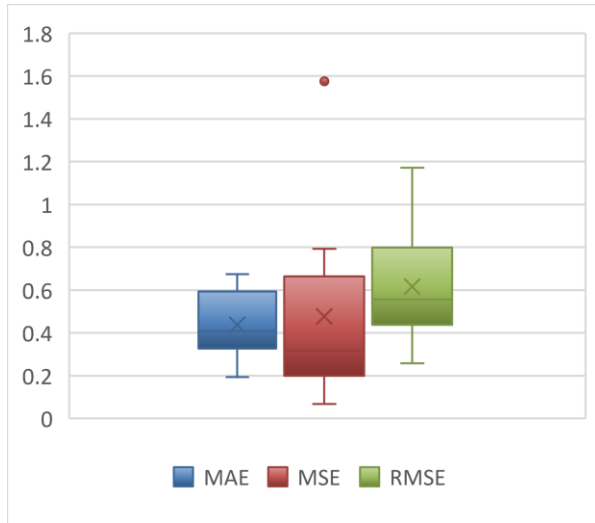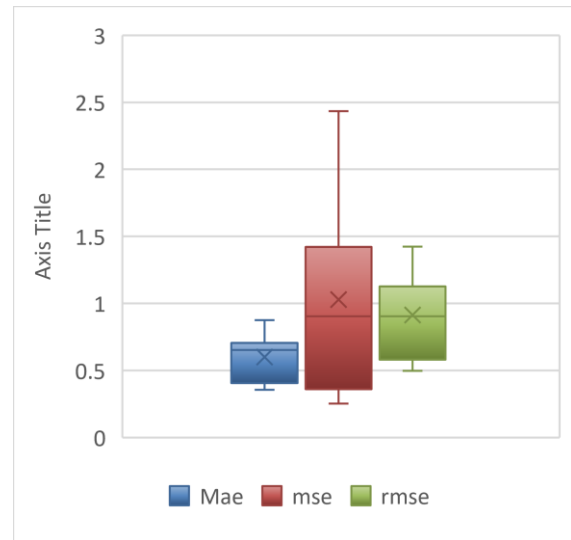**Figure 4.24** Performance Metrics for MNN in iEMG-Based Force Prediction

4.1.7 BPNN

The Backpropagation Neural Network (BPNN) employed for force prediction based on surface electromyography (sEMG) and intramuscular electromyography (iEMG) signals has exhibited varied performance, as outlined in Figures 48 and 49. The model's effectiveness is characterized by key evaluation metrics, shedding light on its ability to accurately predict force dynamics.

For sEMG-based force prediction, the BPNN demonstrated a range of performance metrics. The Mean Absolute Error (MAE) varied from 0.21 to 0.84, indicating the model's ability to make predictions with varying degrees of accuracy. The Mean Squared Error (MSE) values ranged from 0.07 to 1.19, and the Root Mean Square Error (RMSE) values consistently varied from 0.27 to 1.08. The Coefficient of Determination (R^2) values ranged from 0.68 to 0.93, indicating a moderate to strong correlation between the predicted and actual force values derived from sEMG signals.

Turning to iEMG-based force prediction, the BPNN showcased a similar spectrum of performance. The MAE for iEMG predictions ranged from 0.35 to 0.98, showcasing variations in accuracy. The MSE values varied between 0.37 and 1.58, while the RMSE values consistently ranged from 0.50 to 1.25. The Coefficient of Determination (R2) values for iEMG predictions ranged from 0.67 to

0.82, indicating a moderate correlation between the predicted and actual force values derived from iEMG signals.

It's noteworthy that the minimum R^2 values observed for both sEMG and iEMG predictions fall below 0.7. While the model exhibits moderate to strong correlations, the minimum R2 suggests that the BPNN may have limitations in explaining a significant portion of the variability in the actual force values. A value below 0.7 could indicate that the model might not perform optimally in capturing complex relationships within the electromyography data for force prediction.

Figure 4.25 Performance Metrics for BPNN in sEMG-Based Force Prediction

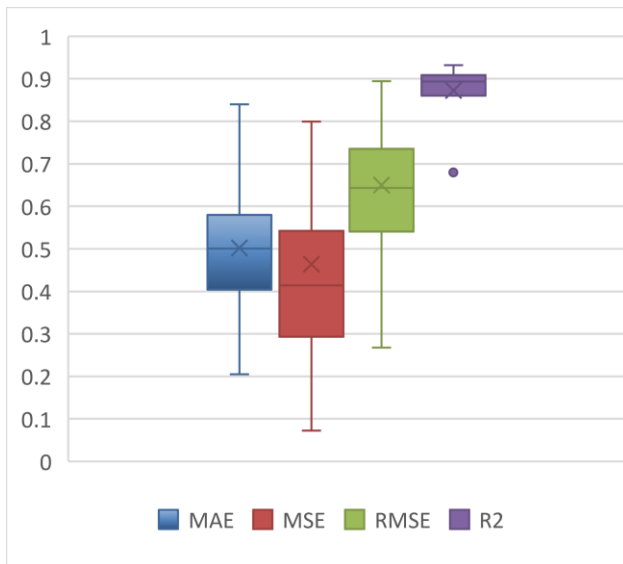**Figure 4.26** Performance Metrics for BPNN in iEMG-Based Force Prediction

4.1.8 Narrow Neural Network

The Narrow Neural Network, utilized for predicting force based on surface electromyography (sEMG) and intramuscular electromyography (iEMG) signals, reveals varied performance metrics as depicted in Figures 4.25 and 4.26. These metrics provide insights into the model's accuracy in predicting force dynamics.

For sEMG-based force prediction, the Narrow Neural Network demonstrates a range of performance metrics. The Mean Absolute Error (MAE) varies from 0.19 to 0.62, indicating the model's capability to make predictions with varying degrees of accuracy. The Mean Squared Error (MSE) values range from 0.06 to 1.15, and the Root Mean Square Error (RMSE) consistently

varies from 0.25 to 1.00. The Coefficient of Determination (R^2) values range from 0.62 to 0.94, suggesting a moderate to strong correlation between the predicted and actual force values derived from sEMG signals.
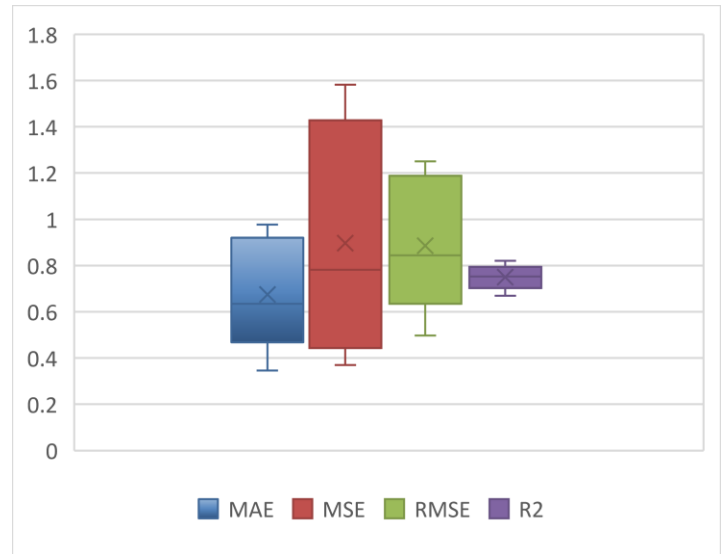
Turning to iEMG-based force prediction, the Narrow Neural Network demonstrates a similar spectrum of performance. The MAE for iEMG predictions ranges from 0.31 to 0.80, showcasing variations in accuracy. The MSE values vary between 0.20 and 1.64, while the RMSE consistently ranges from 0.44 to 1.18. The Coefficient of Determination (R^2) values for iEMG predictions range from 0.62 to 0.86, indicating a moderate correlation between the predicted and actual force values derived from iEMG signals.

While the model's performance metrics indicate a moderate to strong correlation for both sEMG and iEMG predictions, the minimum R^2 values, specifically 0.62, suggest that there may be room for improvement in explaining variability for more robust force predictions. Further exploration and optimization could enhance the model's ability to capture complex relationships within the electromyography data.

Figure 4.27 Performance Metrics for NNN in sEMG-Based Force Prediction
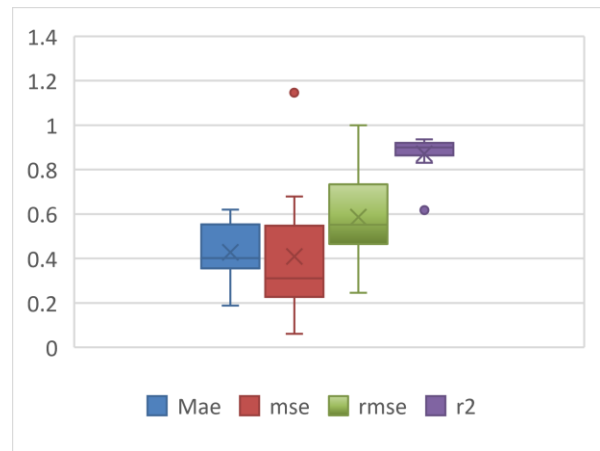
Figure 4.28 Performance Metrics for NNN in sEMG-Based Force Predictio
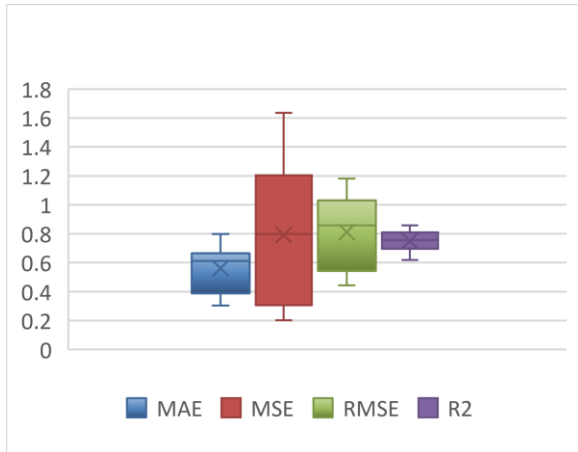
4.1.9 Cubic Support Vector Machine

The performance of the Cubic Support Vector Machine (SVM) in predicting force based on surface electromyography (sEMG) and intramuscular electromyography (iEMG) signals is detailed in

51

Figures 4.29-4.31. The model's effectiveness is reflected in various performance metrics, providing insights into its accuracy in capturing force dynamics.

For sEMG-based force prediction, the Cubic SVM exhibits a range of performance metrics. The Mean Absolute Error (MAE) varies from 0.18 to 0.83, showcasing the model's varying degrees of accuracy in predictions. The Mean Squared Error (MSE) values range from 0.06 to 1.54, and the Root Mean Square Error (RMSE) consistently varies from 0.24 to 2.42. Interestingly, the Coefficient of Determination (R^2) values range from -2.55 to 0.94, indicating a broad spectrum of correlation, with negative values suggesting a poor fit of the model to the data.

Turning to iEMG-based force prediction, the Cubic SVM demonstrates a similar spectrum of performance. The MAE for iEMG predictions ranges from 0.33 to 0.88, showcasing variations in accuracy. The MSE values vary between 0.28 and 17.54, while the RMSE consistently ranges from 0.52 to 2.42. The Coefficient of Determination (R^2) values for iEMG predictions range from -2.55 to 0.83.

The average R^2 values for sEMG and iEMG, calculated as 0.112 and 0.534, respectively, further emphasize the model's limitations in capturing the underlying patterns in the data. These low average R2 values suggest that the Cubic SVM may not be an effective model for predicting force dynamics based on electromyography signals, as the correlation between predicted and actual force values is notably weak. In summary, the Cubic SVM exhibits a wide range of performance for both sEMG and iEMG-based force predictions, with notably low average R^2 values. These findings indicate that the model may not be the most suitable for capturing the intricate relationships within the electromyography data for accurate force predictions. Further exploration and consideration of alternative models may be beneficial to improve predictive capabilities.
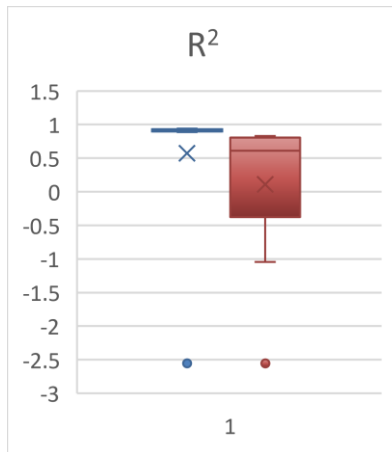
Figure 4.29 R^2 for cSVM in EMG-Based Force Prediction
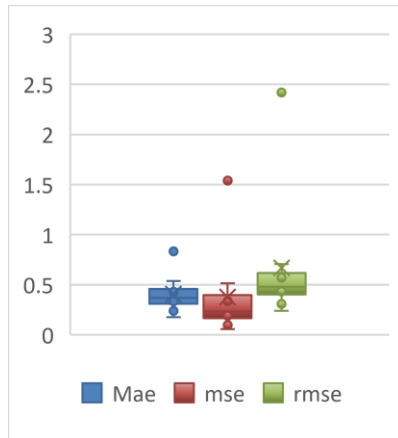
Figure 4.30 Performance Metrics for cSVM in sEMG-Based Force Prediction
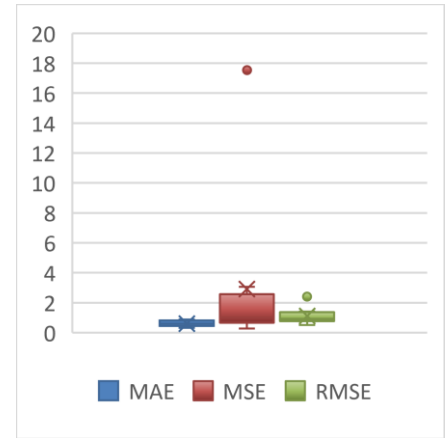
Figure 4.31 Performance Metrics for cSVM in iEMG-Based Force Prediction

4.2 Amputees

4.2.1 Temporal Convolutional Networks

The force prediction using Temporal Convolutional Networks (TCN) in amputee subjects, using surface electromyography (sEMG) signals, exhibits promising results, as illustrated in Figures 4.32 and 4.33. Examining various evaluation metrics, the average Mean Absolute Error (MAE) is 1.31, indicating the model's accuracy in predicting force values. The Mean Squared Error (MSE) averages 5.64, reflecting the overall squared differences between predicted and actual force values. The Root Mean Square Error (RMSE) provides an average measure of prediction accuracy of 1.76. Notably, the Coefficient of Determination (R^2) reaches an average value of 0.87, indicating a robust correlation between predicted and actual force values.

Breaking down further, the minimum MAE is observed at 0.45, reflecting instances of particularly accurate predictions. The minimum MSE and RMSE are 0.57 and 0.61, respectively, signifying low overall prediction errors. The minimum R^2 value is 0.81, indicating a strong relationship between predicted and actual force values in the least favorable scenarios.

Conversely, the model's maximum performance metrics exhibit its capacity to handle variations in force prediction. The maximum MAE is 1.92, representing the largest absolute errors in

prediction. The maximum MSE is 9.37, and the maximum RMSE is 2.50, suggesting instances of higher prediction errors. However, even under these conditions, the model maintains a commendable performance, highlighted by the maximum R^2 value of 0.93, showcasing a substantial correlation between predicted and actual force values.
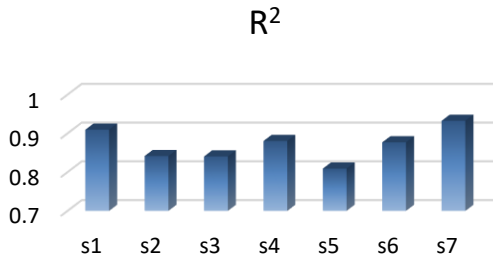
Figure 4.32 R^2 of TCN-based sEMG Force Prediction for Amputees.
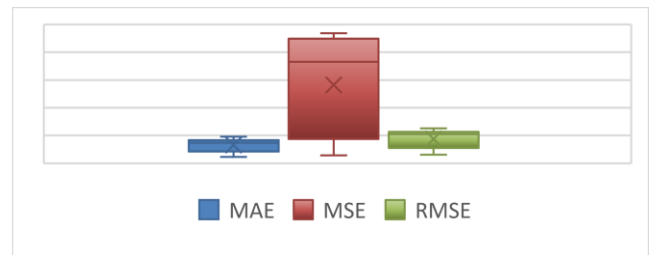
Figure 4.33 Performance Metrics of TCN-based sEMG Force Prediction for Amputee

4.2.2 *LSTM_TCN*

The illustration of LSTM-TCNN model results on the sEMG dataset is presented in Figures 4.34 and 4.35. These metrics offer valuable insights into the model's accuracy in predicting force dynamics.

For sEMG-based force prediction, the LSTM-TCNN demonstrates notable performance metrics. The Mean Absolute Error (MAE) ranges from 0.3229 to 1.4521, indicating the model's capability to make predictions with varying degrees of accuracy. The Mean Squared Error (MSE) values span from 0.3905 to 12.6173, while the Root Mean Square Error (RMSE) consistently varies from 0.4605 to 2.3174. The Coefficient of Determination (R^2) values range from 0.6842 to 0.9344, suggesting a strong correlation between the predicted and actual force values derived from sEMG signals.

The LSTM-TCNN's overall performance metrics indicate its ability to capture complex relationships within the sEMG data for accurate force predictions. The minimum R2 values, specifically 0.6842, suggest room for improvement in explaining variability for more robust force predictions. Further exploration and optimization could enhance the model's ability to capture intricate patterns within the electromyography data.
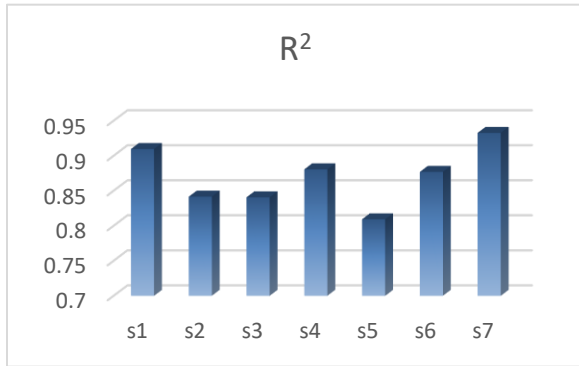
Figure 4.34 R^2 of TCN-based sEMG Force Prediction for Amputees.

Figure 4.35 Performance Metrics of TCN-based sEMG Force Prediction for Amputees

4.2.3 LSTM

The LSTM model, applied to predict force based on surface electromyography (sEMG) signals, is elucidated through performance metrics in Figures 4.36 and 4.37. These metrics offer comprehensive insights into the model's accuracy in forecasting force dynamics.

For sEMG-based force prediction, the LSTM model demonstrates varied performance metrics. The Mean Absolute Error (MAE) spans from 0.3369 to 1.7162, highlighting the model's capacity for predictions with differing levels of accuracy. Mean Squared Error (MSE) values range from 0.4004 to 13.6549, while Root Mean Square Error (RMSE) consistently varies from 0.4816 to 2.4411. Coefficient of Determination (R^2) values range from 0.5848 to 0.9374, suggesting a strong correlation between the predicted and actual force values derived from sEMG signals.

The LSTM model's overall performance metrics indicate its ability to capture intricate patterns within the sEMG data for accurate force predictions. The minimum R^2 value, specifically 0.5848, suggests opportunities for improvement in explaining variability for more robust force predictions. Further exploration and optimization could enhance the model's ability to discern complex relationships within the electromyography data.
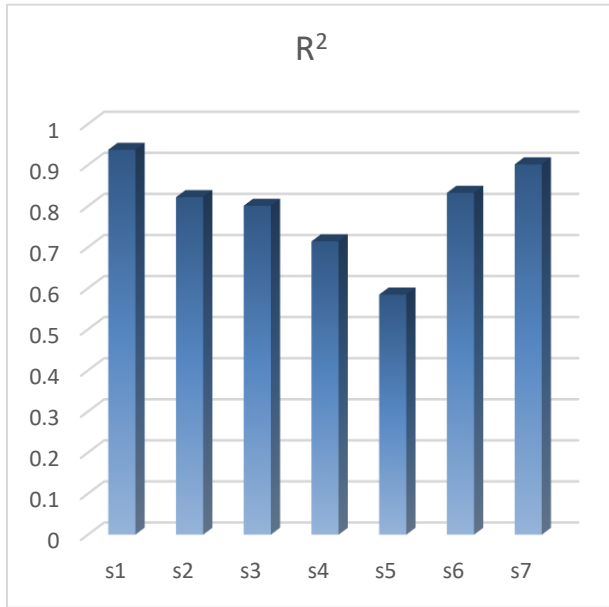
Figure 4.36 R^2 of LSTM-based sEMG Force Prediction for Amputees.

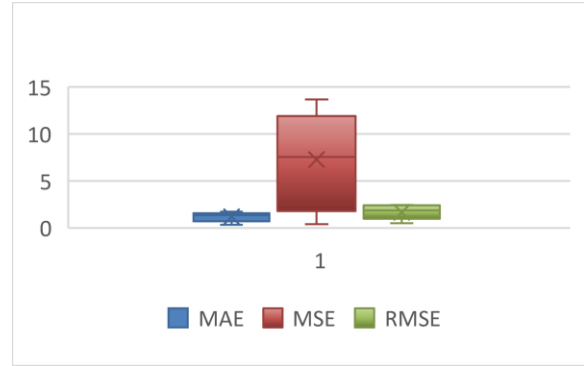**Figure 4.37** Performance Metrics of LSTM-based sEMG Force Prediction for Amputees

4.2.4   Gaussian Process Regression

4.2.3.1   Matern 5/2 kernel

The Gaussian Process Regression (Matern 5/2 kernel), applied to predict force based on surface electromyography (sEMG) signals, is detailed through performance metrics. The following results are illustrated in Figures 4.38 and 4.39.

For sEMG-based force prediction, the model demonstrates consistent performance metrics. The Mean Absolute Error (MAE) averages at 0.8792, ranging from 0.3207 to 1.2197, indicating the model's capability to provide accurate predictions with varying degrees of precision. The Mean Squared Error (MSE) has an average value of 3.6164, with values ranging from 0.3780 to 6.4235, and the Root Mean Square Error (RMSE) consistently varies from 0.6056 to 2.3979. The Coefficient of Determination (R^2) values range from 0.7175 to 0.8961, suggesting a strong correlation between the predicted and actual force values derived from sEMG signals.

The Matern 5/2 kernel's overall performance metrics underscore its ability to capture complex relationships within the sEMG data for accurate force predictions. The minimum R^2 value, specifically 0.7175, implies that the model performs well, and further refinement could potentially

enhance its explanatory power. These findings provide a comprehensive overview of the Gaussian Process Regression with Matern 5/2 kernel in the context of sEMG-based force prediction.

4.2.3.1 Exponential kernel

The Gaussian Process Regression with an exponential kernel, employed for predicting force based on surface electromyography (sEMG) signals, is characterized by the following performance metrics. The results are elucidated in Figures 4.40 and 4.41.
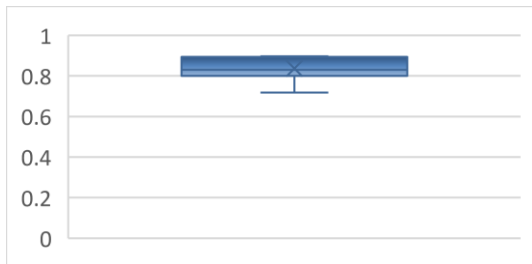
Figure 4.38 R2 of Gpr(mat)-based sEMG Force Prediction for Amputees.
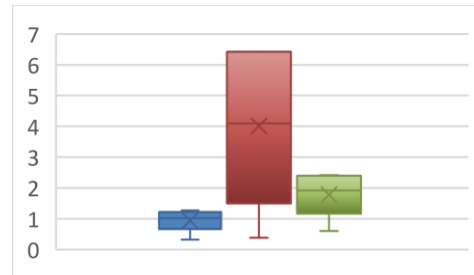
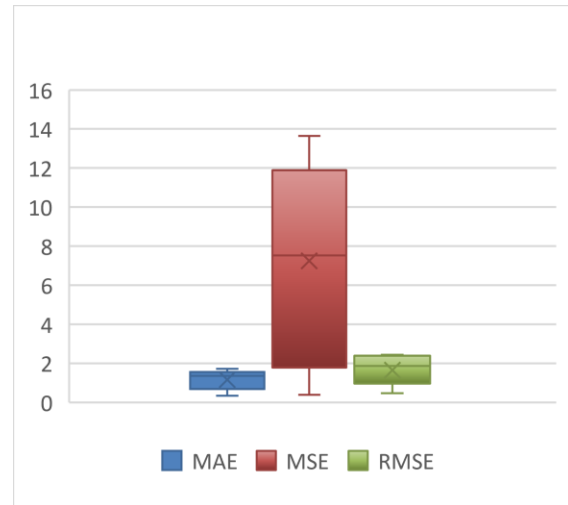**Figure 4.39** Performance Metrics of Gpr(mat)-based sEMG Force Prediction for Amputees.

For sEMG-based force prediction, the Gaussian Process Regression with an exponential kernel exhibits varied performance metrics. The Mean Absolute Error (MAE) averages at 1.1328, with values ranging from 0.3917 to 1.7864. This indicates the model's capability to make predictions with varying degrees of accuracy. The Mean Squared Error (MSE) has an average value of 9.5532, ranging from 0.8888 to 23.3377, and the Root Mean Square Error (RMSE) consistently varies from 0.9203 to 4.7869. The Coefficient of Determination (R^2) values range from 0.3729 to 0.8679, suggesting a moderate to strong correlation between the predicted and actual force values derived from sEMG signals.

The overall performance metrics of the Gaussian Process Regression with an exponential kernel underscore its ability to capture intricate relationships within the sEMG data for force prediction. The minimum R2 value, specifically 0.3729, implies some variability in capturing the underlying patterns, suggesting potential areas for model improvement. These insights contribute to a comprehensive understanding of the Gaussian Process Regression model with an exponential kernel in the context of sEMG-based force prediction.

Figure 4.40 R^2 of Gpr(expo)-based sEMG Force Prediction for Amputees.
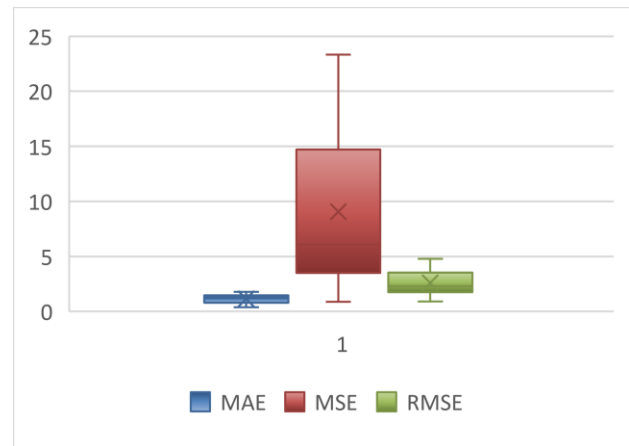
Figure 4.41 Performance Metrics of Gpr(expo)-based sEMG Force Prediction for Amputees.

4.2.5   *Multilayer Perceptron*

The Multilayer Perceptron (MLP) model, utilized for predicting force based on surface electromyography (sEMG) signals, is characterized by various performance metrics as detailed in Figures 4.42 and 4.43. These metrics provide valuable insights into the model's accuracy in forecasting force dynamics.

For sEMG-based force prediction, the MLP model demonstrates consistent performance metrics. The Mean Absolute Error (MAE) averages at 1.0971, ranging from 0.3829 to 1.54. This indicates the model's capability to provide accurate predictions with varying degrees of precision. The Mean Squared Error (MSE) has an average value of 5.3243, with values ranging from 0.4885 to 8.62, and the Root Mean Square Error (RMSE) consistently varies from 0.699 to 2.93. The Coefficient of Determination (R^2) values range from 0.7 to 0.84, suggesting a moderate to strong correlation between the predicted and actual force values derived from sEMG signals.

The MLP model's overall performance metrics highlight its ability to capture complex relationships within the sEMG data for accurate force predictions. The minimum R^2 value, specifically 0.7, implies good explanatory power, while the maximum R^2 of 0.84 indicates strong

correlation under certain conditions. These findings contribute to a comprehensive understanding of the Multilayer Perceptron model in the context of sEMG-based force prediction.
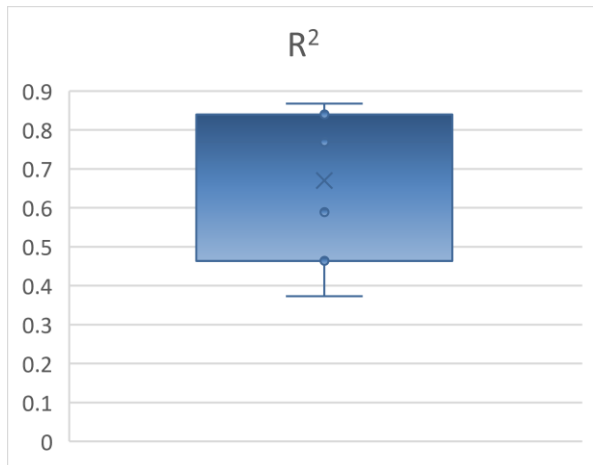

Figure 4.42 R^2 of MLP-based sEMG Force Prediction for Amputees.

Figure 4.43 Performance metrics of MLP-based sEMG Force Prediction for Amputees.

4.2.6   Backpropagation Neural Network

The Backpropagation Neural Network (BPNN) employed for predicting force based on surface electromyography (sEMG) signals is characterized by the following performance metrics. The results are presented in Figures 4.44 and 4.45.

For sEMG-based force prediction, the BPNN exhibits varying performance metrics. The Mean Absolute Error (MAE) averages at 1.8209, with values ranging from 0.7600 to 2.6714. This indicates the model's capability to make predictions with varying degrees of accuracy. The Mean Squared Error (MSE) has an average value of 12.1282, ranging from 1.6226 to 20.4850, and the Root Mean Square Error (RMSE) consistently varies from 1.2738 to 4.5200. The Coefficient of Determination (R^2) values range from 0.4360 to 0.6496, suggesting a moderate correlation between the predicted and actual force values derived from sEMG signals. Given that the minimum R2 value for the Backpropagation Neural Network (BPNN) in the context of sEMG-based force prediction is 0.4360, it suggests that this model may have limitations in accurately capturing the underlying patterns in the data. In situations where force prediction accuracy is crucial, especially for amputee applications requiring precise control, alternative models with higher R^2 values may be more suitable. Therefore, careful consideration and exploration of alternative models are recommended for applications involving amputee users.
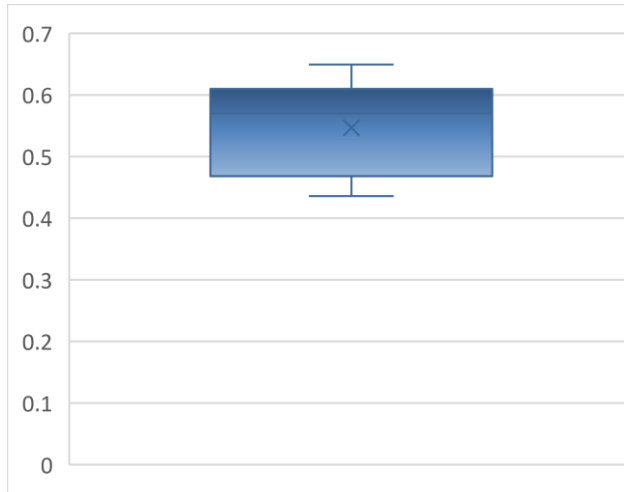
Figure 4.44 R^2 of BPNN-based sEMG Force Prediction for Amputees.

Figure 4.45 Performance metrics of BPNN - based sEMG Force Prediction for Amputees.

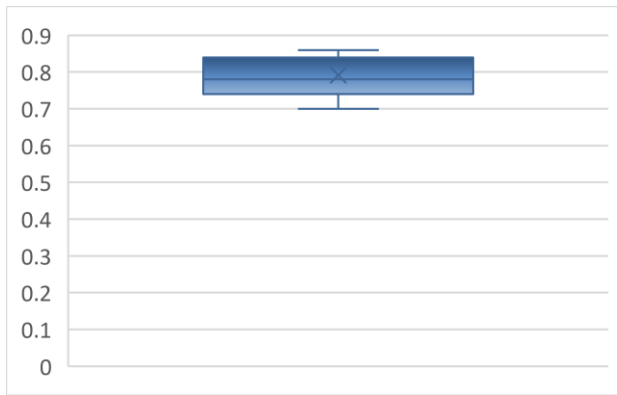### *4.2.7 Medium Neural Network*

The Medium Neural Network, applied for predicting force based on surface electromyography (sEMG) signals, is detailed through performance metrics illustrated in Figures 4.46 and 4.47. These metrics provide insights into the model's accuracy in forecasting force dynamics.
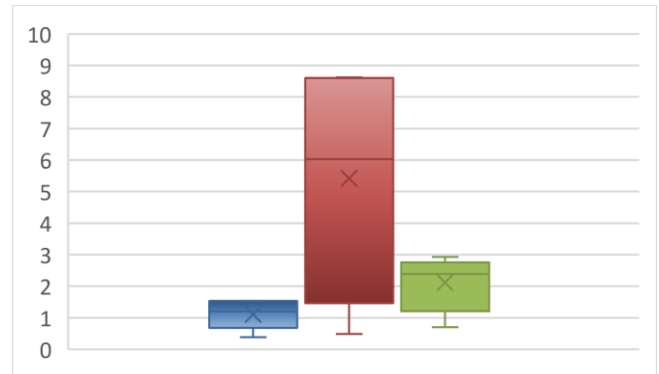
For sEMG-based force prediction, the Medium Neural Network exhibits varied performance metrics. The Mean Absolute Error (MAE) averages at 1.4092, with values ranging from 0.4879 to 2.1206. This indicates the model's capability to make predictions with varying degrees of accuracy. The Mean Squared Error (MSE) has an average value of 7.8218, ranging from 0.6180 to 18.6655, and the Root Mean Square Error (RMSE) consistently varies from 0.7830 to 4.2677. The Coefficient of Determination (R^2) values range from 0.4364 to 0.7736, suggesting a moderate to strong correlation between the predicted and actual force values derived from sEMG signals.

Given that the minimum R^2 value is 0.4364, it is advisable to exercise caution when considering the use of this model for applications involving amputees, where precision in force prediction is crucial. Exploring alternative models with higher R2 values may be recommended for applications requiring enhanced predictive accuracy in amputee-related contexts.

Figure 4.46 R^2 of MNN-based sEMG Force Prediction for Amputees.

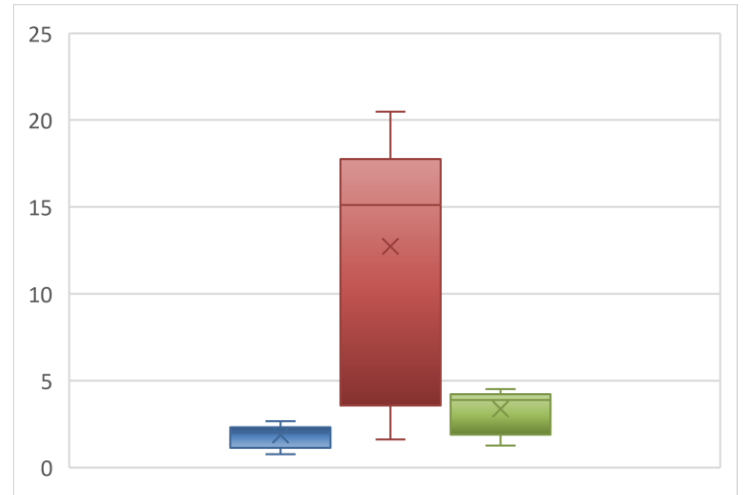**Figure 4.47** Performance metrics of MNN - based sEMG Force Prediction for Amputee

4.2.8   Narrow Neural Network

The performance of the Narrow Neural Network (NNN) in predicting force based on surface electromyography (sEMG) signals is detailed in Figures 4.48 and 4.49. These figures provide a visual representation of the model's performance across various metrics. The model demonstrates varied performance metrics, and the results are presented as follows:

For sEMG-based force prediction, the Narrow Neural Network exhibits diverse performance metrics. The Mean Absolute Error (MAE) averages 1.5012, ranging from 0.4928 to 2.2376, indicating the model's capability to make predictions with varying degrees of accuracy. The Mean Squared Error (MSE) has an average value of 9.3760, ranging from 0.7761 to 17.8217, and the Root Mean Square Error (RMSE) consistently varies from 0.8640 to 3.9796. The Coefficient of Determination (R2) values range from 0.4172 to 0.8202, suggesting a moderate to strong correlation between the predicted and actual force values derived from sEMG signals.

Given the range of R^2 values, it is important to carefully consider the model's performance characteristics. In situations where precise force control is critical, users may want to explore alternative models with higher R^2 values for applications involving amputee users.
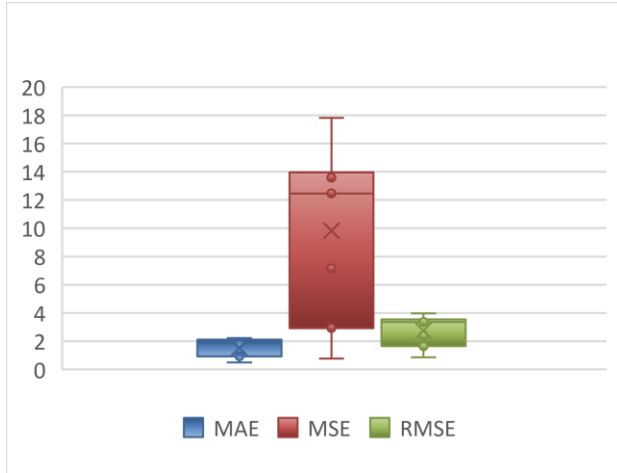
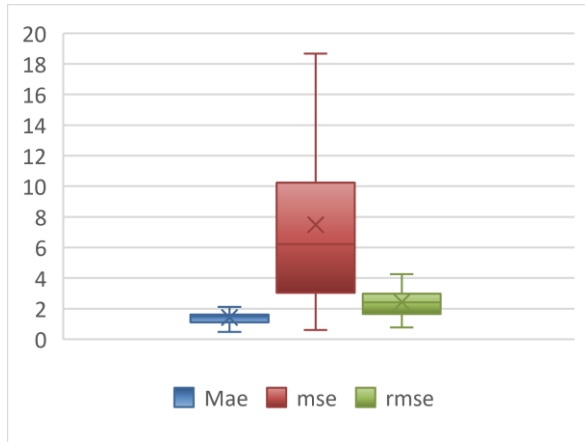**Figure 4.48** R^2 of NNN-based sEMG Force Prediction for Amputees.
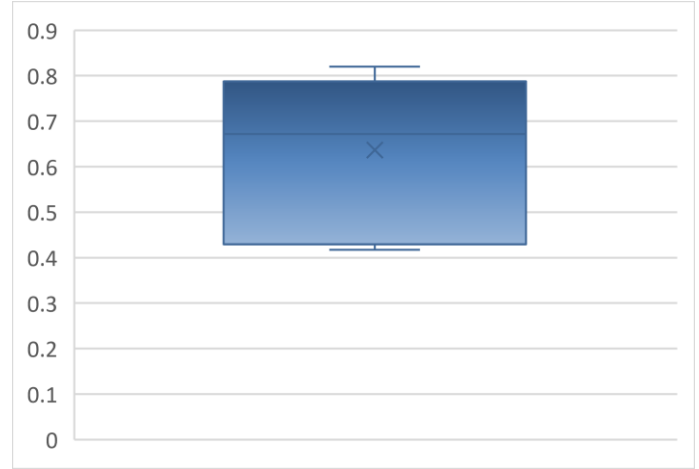
Figure 4.49 Performance metrics of NNN - based sEMG Force Prediction for Amputees
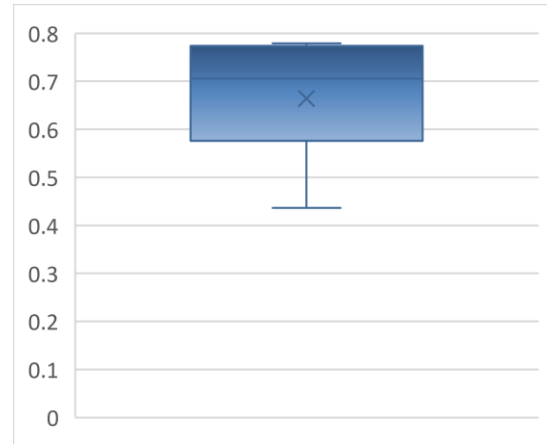
4.2.9   Cubic Support Vector Machine

The performance of the Cubic Support Vector Machine (SVM) in predicting force based on surface electromyography (sEMG) signals is detailed in Figures 4.50 and 4.51. The model's effectiveness is reflected in various performance metrics, providing insights into its accuracy in capturing force dynamics.

For sEMG-based force prediction, the Cubic SVM exhibits varied performance metrics. The Mean Absolute Error (MAE) averages at 1.2562, ranging from 0.4783 to 1.7291, indicating the model's capability to make predictions with varying degrees of accuracy. The Mean Squared Error (MSE) has an average value of 9.5203, ranging from 0.8467 to 14.8519, and the Root Mean Square Error (RMSE) consistently varies from 0.9095 to 3.6696. The Coefficient of Determination (R2) values range from 0.4421 to 0.7794, suggesting a moderate correlation between the predicted and actual force values derived from sEMG signals.

Considering the minimum R^2 value of 0.4421, it indicates that the Cubic SVM may have limitations in explaining variability for more robust force predictions. In the context of applications involving amputee users where precise force control is crucial, alternative models with higher R^2

values may be more suitable. It is advisable to explore and consider alternative models to improve predictive capabilities for such applications.
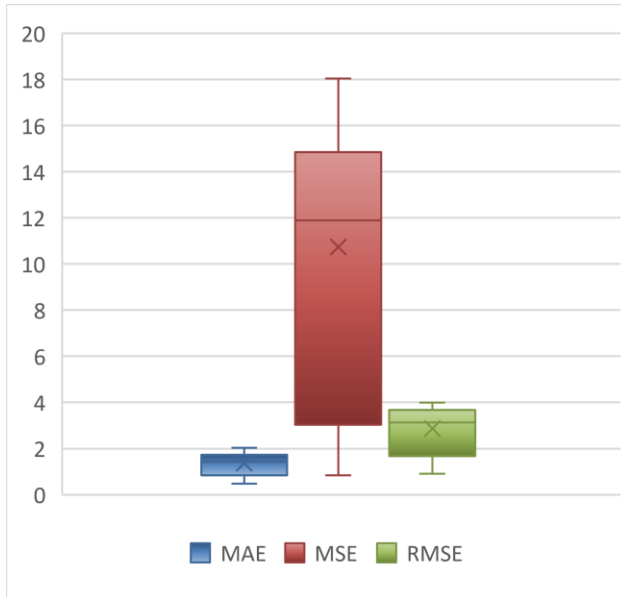
Figure 4.50 R^2 of cSVM-based sEMG Force Prediction for Amputees.
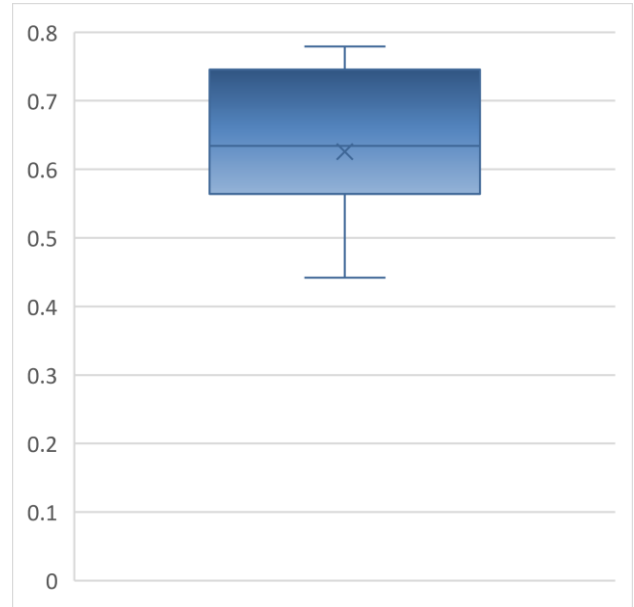
Figure 4.51 Performance metrics of cSVM-based sEMG Force Prediction for Amputee

4.3 Comparison of Surface EMG-Based Force Prediction Models in Amputees

For EMG based force prediction for amputees, the R^2 values obtained from various models serve as key indicators of their predictive performance. The R^2 values quantify how well the models can explain the variability in the force data based on the EMG signals. Among the models assessed, TCN and LSTM_TCN emerge as the top performers, boasting R^2 values of 0.87 and 0.85, respectively. These high R^2 scores suggest that these models excel in capturing the intricate relationships between EMG signals and force predictions for amputees.

The LSTM model also demonstrates commendable predictive capability, yielding an R2 of 0.84. This implies that the LSTM model effectively captures patterns in the EMG data, contributing to accurate force predictions. Additionally, the GPR model with a Matern kernel exhibits competitive performance with an R^2 of 0.84. Conversely, models like GPR with an exponential kernel, MNN, NNN, cSVM, and BPNN show comparatively lower R^2 values ranging from 0.67 to 0.55. While

these models still offer predictive insights, their lower R^2 scores suggest a potential limitation in accurately modeling the relationship between EMG signals and force for amputees. Given that the ANOVA analysis indicates no significant difference among the TCN, LSTM_TCN, LSTM, and GPR with a Matern 5/2 kernel models ($p > 0.05$), it suggests that these models perform similarly in terms of their predictive capabilities for EMG-based force prediction in amputees. In practical terms, this lack of statistical significance implies that the choice between these models may depend on various factors, such as computational efficiency, interpretability, and specific requirements of the application.

TCN, known for its ability to capture long-range dependencies in sequential data, might be favored in scenarios where temporal relationships in the EMG signals play a critical role in force prediction. On the other hand, LSTM_TCN, combining the strengths of both TCN and LSTM, could be a suitable choice when dealing with complex patterns and varying signal lengths. LSTM, with its effectiveness in modeling sequential data, may be preferred when temporal nuances are of utmost importance, especially if interpretability is a key consideration. GPR with a Matern kernel, while statistically on par with the neural network-based models, offers a different approach by providing probabilistic predictions and uncertainty estimates. This could be valuable in applications where understanding the confidence or uncertainty of force predictions is crucial.

Ultimately, the selection among these models should be guided by the specific characteristics of the EMG data, the computational resources available, and the interpretability requirements of the end-users. A well-informed decision, considering the nuances of the amputee dataset and the practical aspects of model deployment, will contribute to the success of the force prediction system in real-world applications.
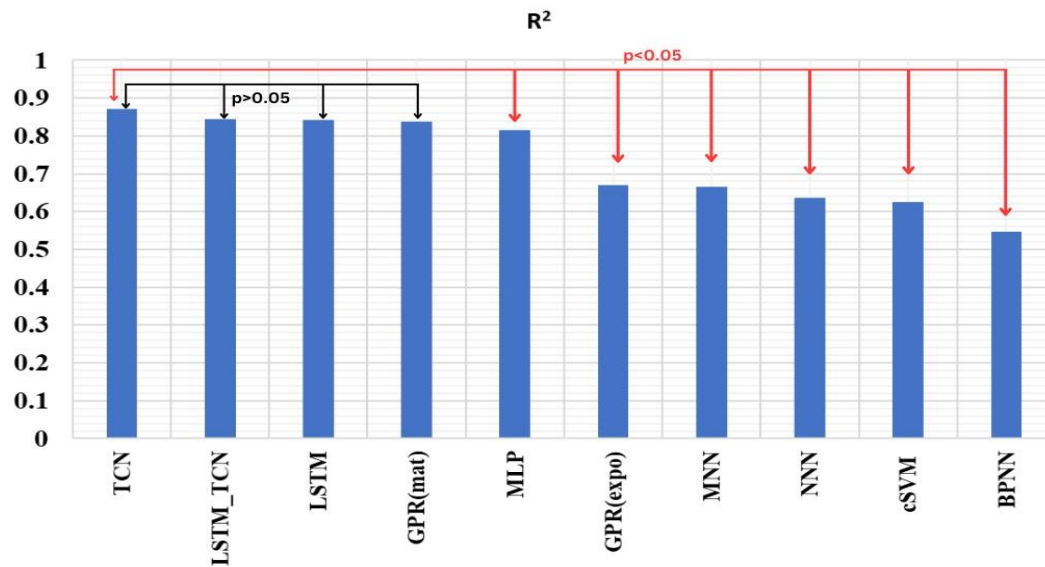
Figure 4.52   Comparison of EMG-Based Force Prediction Models in Amputees

4.1 Comparison of sEMG-Based Force Prediction Models in Able-Bodied

In Figure 4.53, we present the R^2 values for various models in sEMG-based force prediction. Notably, LSTM, LSTM_TCN, and TCN exhibit outstanding performance with R2 values of 0.988, 0.986, and 0.971, respectively, showcasing their exceptional predictive capabilities. GPR (mat) also performs well with an R^2 of 0.938. Among the examined models, LSTM emerges as the frontrunner, attaining an impressive R2 value of 0.988, showcasing its exceptional ability to capture and predict force dynamics accurately. Following closely, LSTM_TCN and TCN exhibit strong performances with R2 values of 0.986 and 0.971, respectively, highlighting their efficacy in handling the complexity of sEMG data.

In the realm of Gaussian Process Regression (GPR), the model with a Matern kernel demonstrates notable predictive power, yielding an R2 value of 0.938. Moving to the other models, GPR with an exponential kernel, MLP, and BPNN exhibit competitive R2 values of 0.937, 0.931, and 0.872, respectively, suggesting their effectiveness in contributing to the predictive accuracy of force dynamics. Meanwhile, NNN, MNN, and cSVM demonstrate R2 values of 0.871, 0.856, and 0.573, respectively, signifying varying degrees of performance across different models. The statistical analysis reveals that LSTM, LSTM_TCN, and TCN models exhibit no significant difference

65

among themselves (p > 0.05), suggesting comparable performance in sEMG-based force prediction. However, their R2 values significantly outshine those of other models in the study. This lack of distinction between the three models underscores their collective superiority and positions them as the most effective choices for accurate force predictions from sEMG signals. Consequently, any one of these models can be confidently employed, offering flexibility in selection based on implementation preferences, computational considerations, or other practical constraints. The robust performance of LSTM, LSTM_TCN, and TCN models underscores their reliability and applicability in enhancing the precision of force prediction tasks in diverse contexts

4.2 Comparison of iEMG-Based Force Prediction Models in Able-Bodied Individuals

Figure 4.54 provides a comprehensive comparison of R2 values obtained from various models utilized for integrated electromyography (iEMG)-based force prediction in able-bodied individuals. Interestingly, the overarching trend in model performances echoes that observed in sEMG-based analyses. Strikingly, LSTM, LSTM_TCN, and TCN models show no significant differences among themselves (p > 0.05), reinforcing their consistently superior performance in both sEMG and iEMG scenarios. Unlike other models, the accuracies of LSTM, LSTM_TCN, and TCN models remain consistent between the two signal types, suggesting their resilience and effectiveness in capturing force dynamics, regardless of the electromyography signal's nature. Notably, the absence of a decrease in accuracy for these deep learning models indicates their adaptability to the unique characteristics of iEMG signals.
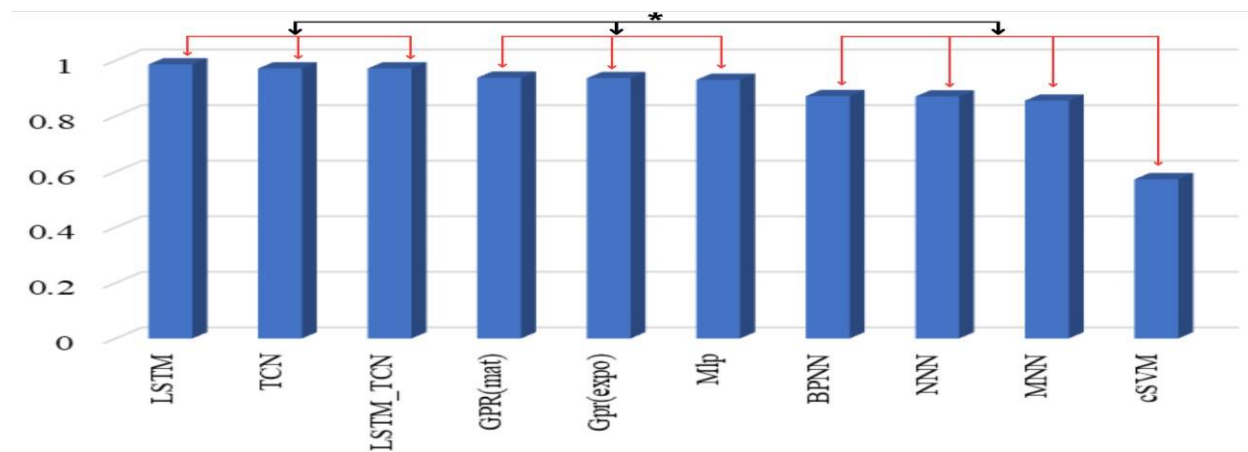
Figure 4.53   Comparison of sEMG-Based Force Prediction Models in Abled bodie

GPR models, including both the exponential and matern kernel variants, continue to exhibit competitive accuracy in iEMG-based force prediction, each securing an R2 value of 0.877. On the other hand, non-deep learning models such as MLP, BPNN, NNN, MNN, and cSVM show a decrease in accuracy, highlighting potential challenges in translating their effectiveness to iEMG data.

In summary, the trio of LSTM, LSTM_TCN, and TCN models stands out as reliable choices for iEMG-based force prediction, showcasing not only consistent performance but also adaptability across different electromyography signal types. This analysis underscores the resilience of deep learning models in maintaining accuracy levels in the transition from sEMG to iEMG contexts, emphasizing their continued efficacy in providing precise force predictions in able-bodied individuals.
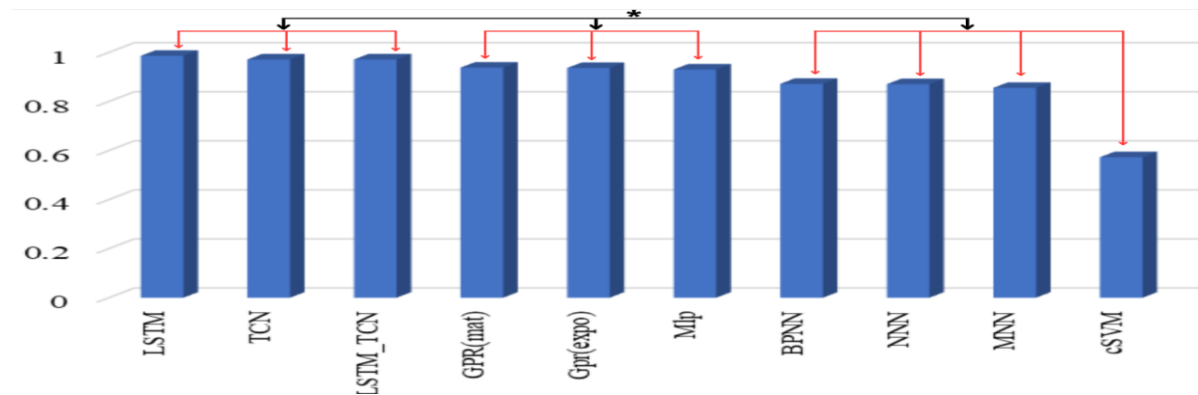
Figure 4.54 Comparison of iEMG-Based Force Prediction Models in Abled bodies

4.3 Comparing sEMG and iEMG-Based Force Prediction Models

The comparison between surface electromyography (sEMG) and integrated electromyography (iEMG) signals for force prediction using various models reveals a consistent trend in model performances, albeit with notable differences in R2 values. Across the board, the models exhibit a similar pattern in their predictive capabilities for both signal types, indicating a degree of generalizability in capturing force dynamics. However, a significant divergence is observed in the R2 values, with a notable decrease in accuracy for most models when transitioning from sEMG to iEMG.

Interestingly, this decrease in accuracy is most pronounced in non-deep learning models such as GPR with an exponential kernel, MLP, BPNN, NNN, MNN, and cSVM. These models demonstrate a diminished ability to effectively capture and predict force dynamics from iEMG signals, suggesting potential challenges in translating their performance from one signal type to another. Contrastingly, deep learning models, including LSTM, TCN, and their hybrid architecture LSTM_TCN, stand out as exceptions to this trend. These models maintain their superior accuracy levels even in the iEMG context, showcasing their robustness and adaptability across different electromyography signal types. This resilience of deep learning architectures highlights their potential for providing accurate force predictions regardless of the unique characteristics inherent in different signal modalities.

In summary, while the overall trend in model performances remains consistent between sEMG and iEMG, the significant decrease in R2 values for most models emphasizes the need for careful consideration and potentially model-specific adaptations when transitioning from one type of electromyography signal to another. The exceptional performance of deep learning models, particularly LSTM, TCN, and LSTM_TCN, underscores their versatility and efficacy in maintaining accurate force predictions across diverse electromyography signal scenarios.

Figure 4.55   Comparison of iEMG and sEMG Based Force Prediction Models in Abled bodied.

SUMMARY OF RESEARCH WORK

This study aimed to assess the effectiveness of various predictive models in estimating force from surface electromyography (sEMG) and integrated electromyography (iEMG) signals. Two distinct datasets were utilized: one from healthy individuals and another from transradial amputees. While the healthy dataset contained simultaneous recordings of sEMG, iEMG, and force, the amputee dataset comprised only sEMG and force data. The analysis of the healthy dataset was split into two parts, focusing separately on force prediction using sEMG-based models and iEMG-based models.

The models evaluated in the study included Temporal Convolutional Networks (TCN), Long Short-Term Memory (LSTM), a hybrid of LSTM and TCN (TCN-LSTM), as well as Cubic Support Vector Machines (SVM), Medium Neural Networks, Narrow Neural Networks, Backpropagation Neural Networks, Multilayer Perceptrons, and Gaussian Process Regression (GPR). The assessment relied on four evaluation metrics: Mean Absolute Error (MAE), Root Mean Squared Error (RMSE), Mean Absolute Percentage Error (MAPE), and the coefficient of determination (R^2). These metrics were used to analyze the performance of the models in predicting force based on both sEMG and iEMG signals for both subject groups.

Results indicated that TCN, LSTM, TCN-LSTM, and GPR exhibited superior performance compared to the other models in predicting force from both sEMG and iEMG signals, irrespective of subject type. Notably, while GPR demonstrated lower performance compared to deep learning networks (LSTM, TCN, TCN-LSTM), it still achieved satisfactory results, with an R^2 higher than 0.8 in healthy individuals and 0.7 in amputees. Additionally, computational cost analysis revealed varying processing times among the models. LSTM required the longest processing time, averaging approximately 70 minutes per subject, while TCN demonstrated significantly faster processing times, ranging from 3 to 5 minutes per subject. GPR, on the other hand, completed computations in less than a minute. These findings underscore the importance of considering both predictive accuracy and computational efficiency when selecting models for force prediction tasks based on electromyography signals.

CHAPTER 5: CONCLUSIONS AND FUTURE RECOMMENDATION

The comparison between surface electromyography (sEMG) and integrated electromyography (iEMG) signals for force prediction using various models reveals a consistent trend in model performances, albeit with notable differences in R^2 values. Across the board, the models exhibit a similar pattern in their predictive capabilities for both signal types, indicating a degree of generalizability in capturing force dynamics. However, a significant divergence is observed in the R^2 values, with a notable decrease in accuracy for most models when transitioning from sEMG to iEMG.

Interestingly, this decrease in accuracy is most pronounced in non-deep learning models such as GPR with an exponential kernel, MLP, BPNN, NNN, MNN, and cSVM. These models demonstrate a diminished ability to effectively capture and predict force dynamics from iEMG signals, suggesting potential challenges in translating their performance from one signal type to another. Contrastingly, deep learning models, including LSTM, TCN, and their hybrid architecture LSTM_TCN, stand out as exceptions to this trend. These models maintain their superior accuracy levels even in the iEMG context, showcasing their robustness and adaptability across different electromyography signal types. This resilience of deep learning architectures highlights their potential for providing accurate force predictions regardless of the unique characteristics inherent in different signal modalities.

In summary, while the overall trend in model performances remains consistent between sEMG and iEMG, the significant decrease in R^2 values for most models emphasizes the need for careful consideration and potentially model-specific adaptations when transitioning from one type of electromyography signal to another. The exceptional performance of deep learning models, particularly LSTM, TCN, and LSTM_TCN, underscores their versatility and efficacy in maintaining accurate force predictions across diverse electromyography signal scenarios.

The study undertook a comprehensive analysis comparing electromyography (EMG)-based and integrated EMG (iEMG)-based force prediction models, revealing a lack of significant difference in performance (P=0.210). This indicates that both methodologies

are equally effective in capturing muscle activity, showcasing their versatility across different user groups, including both abled bodies and amputees. Despite disparities in computational cost, with LSTM exhibiting the longest processing time of approximately 70 minutes per subject, practitioners have the flexibility to choose models based on factors such as computational efficiency without compromising predictive accuracy. This insight underscores the importance of understanding computational cost variations for informed model selection, striking a balance between performance and resource requirements. Notably, Gaussian process regression (GPR), while slightly underperforming compared to other models, still yielded satisfactory results, boasting R2 values exceeding 0.8 in abled-bodied individuals and 0.7 in amputees.

However, the study is not without its limitations. It highlights the need for further research utilizing iEMG signals due to their potential to reduce crosstalk, which could enhance the accuracy of force prediction models. Additionally, there is a call for broader investigations encompassing diverse populations with various neuromuscular disorders and different types of amputations. While the current research focused on healthy individuals and transradial amputees, expanding the scope to include individuals affected by conditions such as cerebral palsy or stroke would provide a more comprehensive understanding of the models' applicability and effectiveness across diverse clinical scenarios.

Furthermore, the study suggests exploring real-time applications of these force prediction models and investigating how external factors might influence the accuracy of force estimation. This avenue of research holds promise for advancing the practical implementation of EMG-based models in clinical settings and assistive device design. By examining real-world scenarios and accounting for external variables, future studies can enhance the robustness and reliability of these predictive models, ultimately improving their utility in assisting individuals with movement disabilities.

In conclusion, the findings of this study offer valuable insights into the practical implementation of EMG-based force prediction models. Despite certain limitations, such as the need for further research on iEMG signals and broader investigations involving diverse populations, the study lays a foundation for future research endeavors. By

addressing these limitations and exploring new avenues of inquiry, researchers can continue to refine and optimize EMG-based force prediction models, ultimately enhancing their effectiveness and applicability in clinical practice and assistive device development.

REFERENCES

[1] Staudenmann, Didier, et al. "Methodological aspects of SEMG recordings for force estimation–a tutorial and review." Journal of electromyography and kinesiology 20.3 (2010): 375-387.

[2] Inman, Verne T., et al. "Relation of human electromyogram to muscular tension." Electroencephalography and clinical neurophysiology 4.2 (1952): 187-194.

[3] Hajian, Gelareh, Ali Etemad, and Evelyn Morin. "Generalized EMG-based isometric contact force estimation using a deep learning approach." Biomedical Signal Processing and Control 70 (2021): 103012.

[4] Hill, Archibald Vivian. "The heat of shortening and the dynamic constants of muscle." Proceedings of the Royal Society of London. Series B-Biological Sciences 126.843 (1938): 136-195.

[5] Mountjoy, Katherine, Evelyn Morin, and Keyvan Hashtrudi-Zaad. "Use of the fast orthogonal search method to estimate optimal joint angle for upper limb Hill-muscle models." IEEE transactions on biomedical engineering 57.4 (2009): 790-798.

[6] Romero, F., and F. J. Alonso. "A comparison among different Hill-type contraction dynamics formulations for muscle force estimation." Mechanical Sciences 7.1 (2016): 19-29.

[7] Lloyd, David G., and Thor F. Besier. "An EMG-driven musculoskeletal model to estimate muscle forces and knee joint moments in vivo." Journal of Biomechanics 36.6 (2003): 765-776.

[8] Buchanan, Thomas S., et al. "Neuromusculoskeletal modeling: estimation of muscle forces and joint moments and movements from measurements of neural command." Journal of Applied Biomechanics 20.4 (2004): 367-395.

[9] Ameri, Ali, et al. "Regression convolutional neural network for improved simultaneous EMG control." Journal of neural engineering 16.3 (2019): 036015. Hajian, Gelareh, et al. "Improving wrist force estimation with surface EMG during isometric contractions." *CMBES Proceedings* 41 (2018).

[10] Hashemi, Javad, et al. "Enhanced dynamic EMG-force estimation through calibration and PCI modeling." *IEEE Transactions on Neural Systems and Rehabilitation Engineering* 23.1 (2014): 41-50.

[11] Martinez, Itzel Jared Rodriguez, et al. "Grasp force estimation from the transient EMG using high-density surface recordings." *Journal of Neural Engineering* 17.1 (2020): 016052.

[12] Bai, Fengjun, and Chee-Meng Chew. "Muscle force estimation with surface EMG during dynamic muscle contractions: A wavelet and ANN-based approach." *2013 35th annual International Conference of the ieee Engineering in medicine and Biology Society (EMBC)*. IEEE, 2013.

[13] Huang, Chengjun, et al. "An isometric muscle force estimation framework based on a high-density surface EMG array and an NMF algorithm." *Journal of Neural Engineering* 14.4 (2017): 046005.

[14] J. Luo, C. Liu, and C. Yang, "Estimation of EMG-Based Force Using a Neural-Network-Based Approach," in IEEE Access, vol. 7, pp. 64856-64865, 2019, doi: 10.1109/ACCESS.2019.2917300.

[15] Hayashibe, M., Guiraud, D. Voluntary EMG-to-force estimation with a multi-scale physiological muscle model. *BioMed Eng OnLine* **12**, 86 (2013). https://doi.org/10.1186/1475-925X-12-86

[16] W. Meng, B. Ding, Z. Zhou, Q. Liu, and Q. Ai, "An EMG-based force prediction and control approach for robot-assisted lower limb rehabilitation," 2014 IEEE International Conference on Systems, Man, and Cybernetics (SMC), San Diego, CA, USA, 2014, pp. 2198-2203, doi: 10.1109/SMC.2014.6974250.

[17] W. Meng, B. Ding, Z. Zhou, Q. Liu and Q. Ai, "An EMG-based force prediction and control approach for robot-assisted lower limb rehabilitation," 2014 IEEE International Conference on Systems, Man, and Cybernetics (SMC), San Diego, CA, USA, 2014, pp. 2198-2203, doi: 10.1109/SMC.2014.6974250.

[18] Wu, Changcheng, et al. "Grip force and 3D push-pull force estimation based on sEMG and GRNN." Frontiers in Neuroscience 11 (2017): 343.

[19] Gui, Kai, Honghai Liu, and Dingguo Zhang. "A practical and adaptive method to achieve EMG-based torque estimation for a robotic exoskeleton." IEEE/ASME Transactions on Mechatronics 24.2 (2019): 483-494.

[20] Hashemi, Javad, et al. "Surface EMG force modeling with joint angle based calibration." *Journal of Electromyography and Kinesiology* 23.2 (2013): 416-424.

[21] Cao, Hongxin, Shouqian Sun, and Kejun Zhang. "Modified EMG-based handgrip force prediction using extreme learning machine." *Soft computing* 21 (2017): 491-500.

[22] Zheng, Yang, and Xiaogang Hu. "Real-time isometric finger extension force estimation based on motor unit discharge information." *Journal of neural engineering* 16.6 (2019): 066006.

[23] Wu, Yansheng, et al. "Difference analysis of musculation and estimation of sEMG-to-force in process of increasing force and decreasing force." Expert Systems with Applications 228 (2023): 120445.

[24] Sakamoto, Sei-ichi, et al. "Ground Reaction Force and Moment Estimation through EMG Sensing Using Long Short-Term Memory Network during Posture Coordination." *Cyborg and Bionic Systems* 4 (2023): 0016.

[25] Mao, He, et al. "Simultaneous estimation of grip force and wrist angles by surface electromyography and acceleration signals." Biomedical Signal Processing and Control 79 (2023): 104088.

[26] Mao, He, et al. "Continuous grip force estimation from surface electromyography using generalized regression neural network." *Technology and Health Care* Preprint (2023): 1-15.

[27] Shirzadi, Mehdi, et al. "A new force profile signal for a convex solution of muscle force estimation from electromyographic signals."

[28] Jiang, Xinyu, Kianoush Nazarpour, and Chenyun Dai. "Explainable and Robust Deep Forests for EMG-Force Modeling." *IEEE Journal of Biomedical and Health Informatics* (2023).

[29] Atzori, Manfredo, et al. "Electromyography data for non-invasive naturally-controlled robotic hand prostheses." *Scientific data* 1.1 (2014): 1-13.

[30] Koiva, Risto, Barbara Hilsenbeck, and Claudio Castellini. "FFLS: An accurate linear device for measuring synergistic finger contractions." *2012 Annual International Conference of the IEEE Engineering in Medicine and Biology Society*. IEEE, 2012.

[31] Na, Youngjin, et al. "A study on estimation of joint force through isometric index finger abduction with the help of SEMG peaks for biomedical applications." IEEE Transactions on Cybernetics 46.1 (2015): 2-8.

[32] M. Nayab, A. Waris, U. Imran, and U. Shafique, "Improving Myoelectric Control Performance through Optimal EMG Signal Feature Selection," 2023 3rd International Conference on Digital Futures and Transformative Technologies (ICoDT2), Islamabad, Pakistan, 2023, pp. 1-5, doi: 10.1109/ICoDT259378.2023.10325706.

[33] Waris, Muhammad Asim, et al. "Classification of functional motions of hand for upper limb prosthesis with surface electromyography." *Int. J. Biol. Biomed. Eng.* 8 (2014): 15-20.

[34] Jochumsen, Mads, Asim Waris, and Ernest Nlandu Kamavuako. "The effect of arm position on the classification of hand gestures with intramuscular EMG." *Biomedical Signal Processing and Control* 43 (2018): 1-8.

[35] Waris, Asim, et al. "A multiday evaluation of real-time intramuscular EMG usability with ANN." *Sensors* 20.12 (2020): 3385.

[36] Saeed, Bushra, et al. "Comparative analysis of classifiers for EMG signals." *2019 IEEE Canadian Conference of Electrical and Computer Engineering (CCECE)*. IEEE, 2019.

[37] Waris, Asim, and Ernest Nlandu Kamavuako. "Effect of threshold values on the combination of EMG time domain features: Surface versus intramuscular EMG." *Biomedical Signal Processing and Control* 45 (2018): 267-273.

[38] Spiewak, Christopher, et al. "A comprehensive study on EMG feature extraction and classifiers." Open Access Journal of Biomedical Engineering and Biosciences 1.1 (2018): 1-10.

[39] Atzori et al., Electromyography data for non-invasive naturally-controlled robotic hand prostheses. Scientific Data, 2014

[40] Bai, Shaojie, J. Zico Kolter, and Vladlen Koltun. "An empirical evaluation of generic convolutional and recurrent networks for sequence modeling. arXiv 2018." *arXiv preprint arXiv:1803.01271* 2 (1803).

[41] Hochreiter, Sepp, and Jürgen Schmidhuber. "Long short-term memory." *Neural Computation* 9.8 (1997): 1735-1780.

LIST OF PUBLICATIONS

- Improving Myoelectric Control Performance through Optimal EMG Signal Feature Selection (doi: 10.1109/ICoDT259378.2023.10325706).

- Examining the Impact of Different K Values on the Performance of Multiple Algorithms in K-Fold Cross-Validation (Doi: 10.1109/ICoDT259378.2023.10325695).

- Surface and Intramuscular Electromyography for Precise Force Prediction in Amputees and Able-Bodied (under review)

- Intelligent Method for Automatic Feature Selection and Dimensionality Reduction for Optimal Control of EMG-Driven Systems (under review)